Redox Biology 62 (2023) 102689

Contents lists available at ScienceDirect

Redox Biology

journal homepage: www.elsevier.com/locate/redox

HIV-1 Tat-mediated microglial ferroptosis involves the miR-204–ACSL4 signaling axis

Muthukumar Kannan [a], Susmita Sil [a], Abiola Oladapo [a], Annadurai Thangaraj [a,b], Palsamy Periyasamy [a,*], Shilpa Buch [a,**]

[a] Department of Pharmacology and Experimental Neuroscience, University of Nebraska Medical Center, Omaha, NE, 68198-5880, USA
[b] Centre for Excellence in Nanobio Translational Research, Department of Pharmaceutical Technology, Anna University, BIT Campus, Tiruchirappalli, Tamil Nadu, 620 024, India

ARTICLE INFO

Keywords:
Microglia
Ferroptosis
HIV-1 Tat
Neuroinflammation
Lipid oxidation

ABSTRACT

This study was focused on exploring the role of the HIV-1 Tat protein in mediating microglial ferroptosis. Exposure of mouse primary microglial cells (mPMs) to HIV-1 Tat protein resulted in induction of ferroptosis, which was characterized by increased expression of Acyl-CoA synthetase long-chain family member 4 (ACSL4), in turn, leading to increased generation of oxidized phosphatidylethanolamine, elevated levels of lipid peroxidation, upregulated labile iron pool (LIP) and ferritin heavy chain-1 (FTH1), decreased glutathione peroxidase-4 and mitochondrial outer membrane rupture. Also, inhibition of ferroptosis by ferrostatin-1 (Fer-1) or deferoxamine (DFO) treatment suppressed ferroptosis-related changes in mPMs. Similarly, the knockdown of ACSL4 by gene silencing also inhibited ferroptosis induced by HIV-1 Tat. Furthermore, increased lipid peroxidation resulted in increased release of proinflammatory cytokines, such as TNFα, IL6, and IL1β and microglial activation. Pretreatment of mPMs with Fer-1 or DFO further blocked HIV-1 Tat-mediated microglial activation *in vitro* and reduced the expression and release of proinflammatory cytokines. We identified miR-204 as an upstream modulator of ACSL4, which was downregulated in mPMs exposed to HIV-1 Tat. Transient transfection of mPMs with miR-204 mimics reduced the expression of ACSL4 while inhibiting HIV-1 Tat-mediated ferroptosis and the release of proinflammatory cytokines. These *in vitro* findings were further validated in HIV-1 transgenic rats as well as HIV + ve human brain samples. Overall, this study underscores a novel mechanism(s) underlying HIV-1 Tat-mediated ferroptosis and microglial activation involving miR-204–ACSL4 signaling.

1. Introduction

The advent of combination antiretroviral therapy (cART) has changed HIV-1 infection from a death sentence to a manageable chronic disease. An estimated 37.7 million people living with HIV-1 (PLWH) worldwide, of which 28.2 million have access to antiretroviral therapy [1]. While cART therapy cannot wholly eliminate HIV-1, it significantly reduces the viral burden and opportunistic infections, remarkably improving the life expectancy of PLWH. Interestingly, despite effective virus suppression, early viral proteins, including the HIV-1 Transactivator of Transcription (Tat), persist in tissues such as the brain and lymph nodes. HIV-1 Tat was first identified as a neurotoxin [2] and is of particular interest owing to its ability to elicit neuroexcitatory responses [3–7]. This protein has gained much attention in the context of HIV-1-associated neurocognitive disorders (HAND) due to its higher expression in the postmortem brain of HIV-1-infected patients [8,9]. HIV-1 Tat primarily enters cells through heparan sulfate proteoglycans, which act as receptors for HIV-1 Tat uptake [10,11]. It is also reported that HIV-1 Tat can penetrate the cell membrane through a non-receptor-mediated transport mechanism [12,13]. After entering the cells, HIV-1 Tat accumulates in endolysosomes and causes lysosomal deacidification. These events subsequently increase the efflux of endolysosomal iron [14,15]. In a state of the excess iron pool, the available free iron produces highly reactive hydroxyl radicals through the Fenton reaction [16,17], further underpins the importance of tight iron control in tissues and cells [18]. Notably, iron is stored in ferritin as a cellular deposit to protect cells from the detrimental effects of the Fenton reaction. Ferritin is a multimeric protein complex composed of heavy and

* Corresponding author.
** Corresponding author.
E-mail addresses: palsamy.periyasamy@unmc.edu (P. Periyasamy), sbuch@unmc.edu (S. Buch).

https://doi.org/10.1016/j.redox.2023.102689
Received 23 February 2023; Received in revised form 20 March 2023; Accepted 26 March 2023
Available online 1 April 2023

light subunits [19,20]. Several studies have suggested a potential link between iron metabolism, oxidative stress, and the progression of HIV-1 infection and pathogenesis [21–24]. A recent clinical study shows that higher levels of iron transport proteins in cerebrospinal fluid are coupled with an increased prevalence of HAND [25].

The brain is vulnerable to oxidative stress because of high levels of polyunsaturated fatty acids [26–28], high levels of redox transition metals [29,30], and high consumption of oxygen for its functioning [31,32]. Free radicals produced during metabolism attack the polyunsaturated fatty acids leading thereby to the generation of highly reactive electrophilic aldehydes such as malondialdehyde (MDA) and 4-hydroxynonenal (4-HNE) [33]. These electrophilic aldehydes are toxic lipid peroxidation products that need to be cleared by the system [34,35]. Cells are equipped with a battery of antioxidants to combat these lipid peroxides. Glutathione peroxidase 4 (GPX4) is one of the antioxidants that quench lipid peroxides in the membrane [36–38]. In HIV-1 patients, MDA was significantly elevated with a concomitant decrease in total antioxidant status [39], suggesting the occurrence of lipid peroxidation and oxidative stress in PLWH. Many studies have reported HIV-1 Tat-mediated production of reactive oxygen species (ROS) followed by lipid peroxidation and increased oxidative stress in various cells [40–44]. HIV-1 Tat can also modulate the functions of CNS cells, including microglia and astrocytes [45–47] and is presumed to be involved in the pathogenesis of HAND and also premature aging [48–53].

Microglia are brain-resident immune cells that can store iron for cellular functions. Microglia also elicit differential sensitivity towards the stress stimuli based on their activation state, i.e., M1 (proinflammatory) or M2 (anti-inflammatory) phenotype. It is well-known that activated M1-microglia secrete several proinflammatory cytokines via dysregulated iron metabolism, increased labile iron pool (LIP), and ROS production [54,55]. A recent study also demonstrated that activated M1-microglia undergo a newly identified type of iron-dependent, oxidative, and non-apoptotic cell death called ferroptosis [56]. The accumulation of intracellular LIP and increased lipid peroxides are critical events in ferroptosis [56]. Microglia also generate selective lipid peroxidation, leading to the pro-ferroptotic signal formation by Acyl-CoA synthetase long-chain family member 4 (ACSL4) [56]. ACSL4 is an enzyme activating polyunsaturated fatty acids, is expressed by all the CNS cells [57], and is found in the mitochondria-associated membrane, mitochondria, endoplasmic reticulum, and peroxisomes [58,59]. Many studies have reported the role of ACSL4 in many biological functions, including inflammation, steroidogenesis, cell death, female fertility, and cancer [60–65].

Many studies have examined the contribution of HIV-1 Tat to neuropathology, including HAND [66]. Iron overload is also a risk factor for the rapid progression of HAND [67] and other neurodegenerative disorders, including Alzheimer's disease, Parkinson's disease, and Huntington's disease [67]. Ferritin heavy chain has been reported to act as a novel intracellular mediator in dendritic damage, thereby contributing to neurocognitive impairments associated with NeuroHIV [68,69]. Despite significant progress made over the years, no previous research has investigated HIV-1 Tat-mediated ferroptosis in microglial cells. The current study provides the first evidence to show that HIV-1 Tat induces ferroptosis in microglial cells and provides evidence that HIV-1 Tat mediates all the signature events of ferroptosis involving decreased expression of GPX4, increased iron levels, increased lipid peroxidation, and rupture of the outer mitochondrial membrane via the miR-204–ACSL4 axis.

2. Material and methods

2.1. Reagents

Deferoxamine (DFO; D9533), Erastin (E7781), and Ferrostatin (Fer-1; SML0583) were purchased from Sigma-Aldrich, St. Louis, MO, USA. BODIPY™ 581/591 C^{11} (Lipid Peroxidation Sensor; D3861) was purchased from ThermoFisher Scientific. TaqMan miR assays for has-miR-204 (Cat No. 000508), TaqMan miR Control Assay U6 snRNA (Cat No. 4427975), miR-204 mimic (Assay ID: MC11116), mirVana™ miRNA mimic, negative control (Cat No. 4464061), ACSL4 siRNA (Assay ID: 122,221) and Silencer™ Negative Control No. 1 siRNA (Cat No. AM4611) was obtained from ThermoFisher Scientific, Inc., Pittsburgh, PA, USA. Antibodies used in this study were procured from these sources: mouse monoclonal anti-GPX4 (Cat No. Sc-166,570; Santa Cruz Biotechnology, Inc., Dallas, TX, USA), rabbit polyclonal anti-FTH1 (Cat No. ab75973; Abcam, Boston, MA, USA), rabbit polyclonal anti-4-HNE (Cat No. ab46545; Abcam, Boston, MA, USA), rabbit monoclonal anti-ACSL4/FACL4 (Cat No. ab205199; Abcam, Boston, MA, USA), rabbit polyclonal anti-CD11b (Cat No. NB110-89474; Novus Biologicals, LLC. Centennial, CO, USA), Anti Iba1, Rabbit, (Cat No. 019–19741; Wako Pure Chemical Industries, Ltd., Irvine, CA, USA), anti-β-Actin-HRP (Cat No. Sc-47778 HRP; Santa Cruz Biotechnology, Inc., Dallas, TX, USA), Peroxidase-AffiniPure Goat Anti-Rabbit IgG (H + L) (Cat No. 111035-003; Jackson ImmunoResearch Inc. West Grove, PA, USA) and Peroxidase-conjugated AffiniPure Goat Anti-Mouse IgG (H + L) (Cat No. 115-035-003; Jackson ImmunoResearch Inc. West Grove, PA, USA).

2.2. Animals

HIV-1 transgenic (Tg) rats and their corresponding age, sex-matched wild-type rats (15 month old male) were used in this study (n = 4/group). Rats were housed as per the Institutional Animal Care and Use Committee protocol (Approval number #18-030-04-FC). The animals were killed, the brain was dissected, and the brain regions were removed and stored at −80 °C.

2.3. Human studies

The human frontal cortex brain sections (donors age range between 45 and 60 years) were received from National NeuroAIDS Tissue Consortium (NNTC), and the details of the human frontal cortex brain sections were published earlier [70]. Briefly, the human frontal cortex brain samples were divided into 2 groups: Group 1 (HIV−ve, n = 3) and Group 2 (HIV + ve, mild neurocognitive disorders, n = 4). Paraffin fixed sections were used for immunostaining of ferroptosis markers such as ACSL4 and 4-HNE. Ten fields from the frontal cortex from each post-mortem human brain sample were used for quantification via Image J Launcher software.

2.4. Mouse primary microglia (mPMs) isolation

mPMs isolation was performed as previously published [71–73]. Briefly, mixed mouse primary glia cultures were prepared from 1 to 3-day C57BL/6 newborn pups. After 9–11 days of culturing, mPMs were collected and seeded on cell culture plates for all experiments.

2.5. Adult rat microglia isolation

We isolated the adult microglia from the wild-type and HIV-1 Tg rats (15-month-old, male) using an Adult Brain Dissociation kit (Cat No. 130-107-677, Miltenyi Biotec Inc. Auburn, CA, USA) as per manufacturer's instructions. Isolated pure adult microglial cells were used for the ferroptosis experiments.

2.6. Lipidomics study

Overnight serum-starved microglial cells were exposed to HIV-1 Tat (100 ng/ml; Cat No. 1032-10; ImmunoDX, Woburn, MA, USA) for 48 h. At the end of the experiment, cells were collected, stored at −80 °C, and then shipped in dry ice to the Southeast Center for Integrated Metabolomics at the University of Florida for lipidomic analysis. The data

generated from positive and negative ion modes were individually examined and normalized using LipidMatch software [74].

2.7. BODIPY™ 581/591 C^{11} imaging

Overnight serum-starved mPMs or ACSL4 siRNA, or miR-204 mimics transfected mPMs, were exposed to HIV-1 Tat, erastin, and other ferroptosis inhibitors for 48 h. After the treatment, C11-BODIPY (2 μM) and 1 μM Hoechst 33,342 (Cat No. H3570; ThermoFisher Scientific, Inc., Pittsburgh, PA, USA) were added and further incubated for 30 min in a CO_2 incubator at 37 °C. After washing with HBSS, fluorescence images were acquired using a Z1 inverted microscope (Carl Zeiss Microscopy, LLC, White Plains, NY, USA).

2.8. Western blotting

After treatment, cell/tissue lysates were used to determine the protein expression levels of ferroptosis markers and microglial activation markers using Western blotting, as per our earlier publications [72,73,75,76].

2.9. Malondialdehyde (MDA) assay

The levels of MDA in mPMs were determined using the Lipid Peroxidation Assay Kit (Cat No. ab118970; Abcam, Boston, MA, USA) as per the manufacturer's instructions.

2.10. Labile iron pool (LIP) quantification

mPMs were cultured in a six-well plate and, after overnight starvation, exposed to HIV-1 Tat as described. mPMs were then lysed using the iron assay buffer, and the levels of total LIP were determined using the iron assay kit (Cat No. ab83366; Abcam, Boston, MA, USA).

2.11. Transmission electron microscopy

Overnight starved mPMs were treated with either HIV-1 Tat (100 ng/ml) or 5 μM erastin for 48 h. After that, cells were harvested, washed, and fixed with EM-grade glutaraldehyde fixative buffer for 30 min. After processing, images were obtained using an FEI Tecnai G2 Spirit transmission electron microscope (FEI, Houston, TX, USA).

2.12. Seahorse cell mito stress test

Oxygen consumption rate (OCR) was measured in mPMs exposed to HIV-1 Tat, erastin, or ferroptosis inhibitors using a Seahorse XFp Extracellular Flux Analyzer as published earlier [47]. The OCR values were analyzed using the Seahorse Wave 2.2.0 (Seahorse Bioscience, Santa Clara, CA, USA).

2.13. TaqMan miR-204 assays

The expression of miR-204 was quantified using TaqMan® miR assays as described earlier [46]. Briefly, total RNA was used in cDNA synthesis with specific miR primers using TaqMan® miR Reverse Transcription kit (Cat No. 4366596; ThermoFisher Scientific, Inc., Pittsburgh, PA, USA). Then the expression level of miR-204 was analyzed by the Applied Biosystems® QuantStudio™ 3 Real-Time PCR System (Applied Biosystems, Grand Island, NY, USA) using TaqMan Universal PCR Master mix, no AmpErase UNG (Cat No. 4324018; ThermoFisher Scientific, Inc., Pittsburgh, PA, USA), using the comparative $2^{-\Delta\Delta Ct}$ method.

2.14. miR-204 overexpression

mPMs were transiently transfected with either miR-204 mimic or miR-control using Lipofectamine™ RNAiMAX (Cat No. 13778150; ThermoFisher Scientific, Inc., Pittsburgh, PA, USA) as described previously [45,46,72,75]. Then the transfected cells were exposed to HIV-1 Tat (100 ng/ml; 48 h) to determine the ferroptosis signaling.

2.15. Quantification of proinflammatory cytokines by qPCR

Isolated total RNA was reverse transcribed using a Verso cDNA Synthesis Kit (Cat No. AB-1453/B; ThermoFisher Scientific, Inc., Pittsburgh, PA, USA) and used for determining the proinflammatory cytokines gene expression. TaqMan probes for TNFα (Mm00443258), IL1β (Mm00434228), IL6 (Mm00446190), and GAPDH (Mm99999915) were purchased from Applied Biosystems, Grand Island, NY. The expression levels of TNFα, IL1β, and IL6 were normalized with GAPDH.

2.16. ACSL4 siRNA transfection

mPMs were transiently transfected with either ACSL4 siRNA or scrambled siRNA using Lipofectamine™ RNAiMAX (Cat No. 13778150; ThermoFisher Scientific, Inc., Pittsburgh, PA, USA) as described previously [45,46,72,75]. Then the transfected cells were exposed to HIV-1 Tat (100 ng/ml; 48 h) to determine the ferroptosis signaling.

2.17. ELISA for proinflammatory cytokines

Cell culture supernatants were collected after HIV-1 Tat exposed mPMs with and without ferroptosis inhibitors and were analyzed for secreted cytokines such as IL1β (Cat No. ab197742, IL6 (Cat No. ab222503), and TNFα (Cat No. ab208348) using the ELISA kit (Abcam, Boston, MA, USA).

2.18. Immunohistochemistry

Immunohistochemistry was performed as previously published [73,76] for determining the expression profile of ferroptosis marker, FTH1, ACSL4, and 4-HNE. After processing, fluorescence images were acquired using a Z1 inverted microscope (Carl Zeiss Microscopy, LLC, White Plains, NY, USA).

2.19. Ago2 immunoprecipitation

Ago2 immunoprecipitation was performed using the miR Target IP Kit (Cat No. 25500; Active Motif, Carlsbad, CA, USA). After the pull-down, RNA extraction was performed using the Phenol: Chloroform method per the manufacturer's instructions. Total and Ago2-immunoprecipitated RNA samples were then used for determining the enrichment of ACSL4 by qPCR.

2.20. Statistical analysis

All the data were expressed as mean ± SD, and appropriate statistical significance was chosen based on the experimental strategy using GraphPad Prism version 9. For multiple group comparisons, nonparametric Kruskal–Wallis one-way ANOVA followed by Dunn's *post hoc* test was used, and for two group comparisons, the Wilcoxon matched-pairs signed rank test was used. An unpaired Student's *t*-test was used to compare two groups for the *in vivo* experiments. Values were statistically significant when $P < 0.05$.

3. Results

3.1. HIV-1 tat-induced lipid oxidation in mPMs

To determine HIV-1 Tat-mediated microglial lipid oxidation, we first sought to determine the expression levels of 4-HNE-modified protein adducts using the 4-HNE antibody [77] in cells exposed to HIV-1 Tat

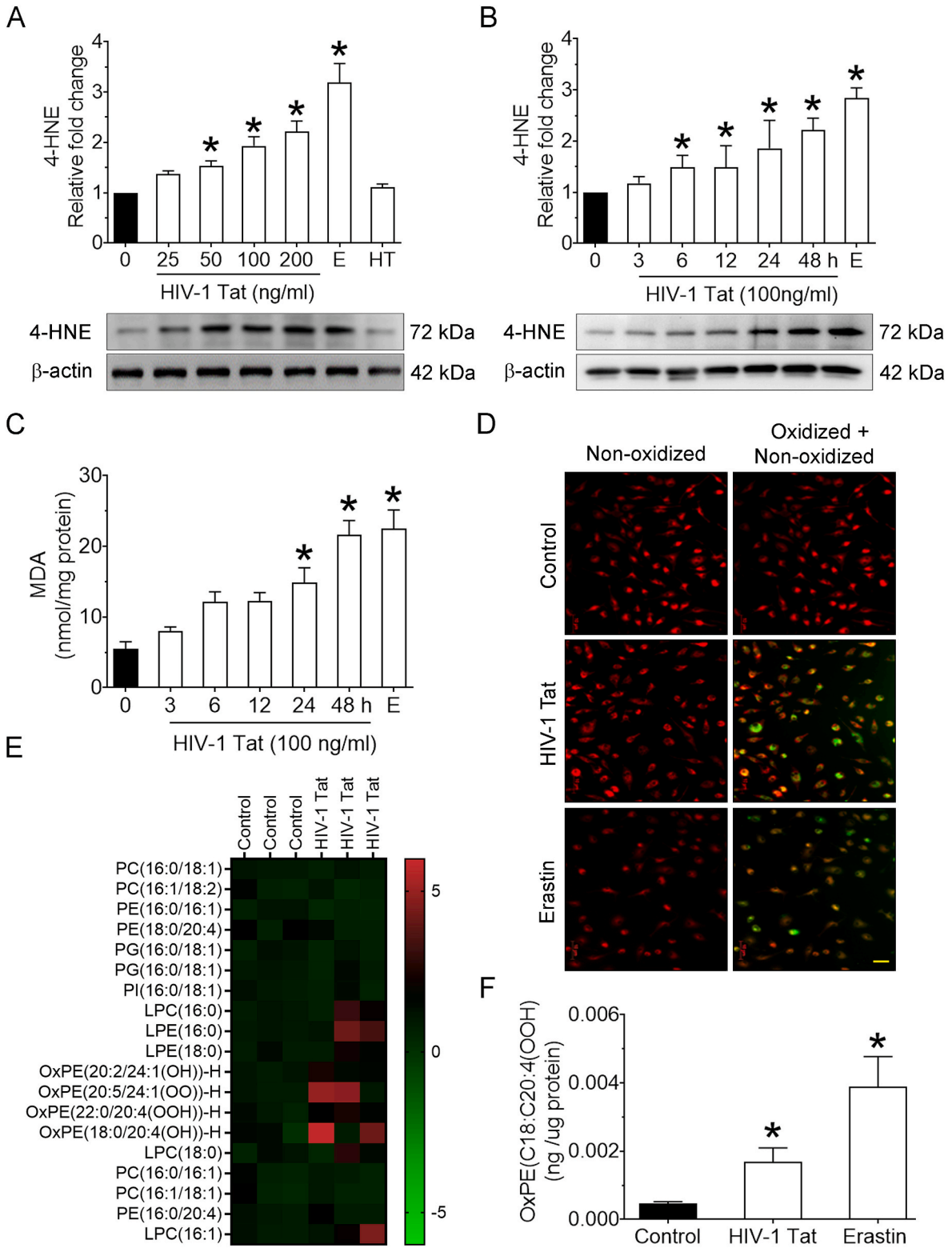

Fig. 1. HIV-1 Tat-induced lipid oxidation in mPMs.
Representative western blotting imaging showing the dose (A) and time (B) dependent expression of 4-HNE in HIV-1 Tat exposed mPMs. β-actin was used as an internal control for all the experiments. Bar graph showing the levels of MDA in HIV-1 Tat exposed mPMs (C). The data are presented as mean ± SD from six independent experiments. Nonparametric Kruskal–Wallis one-way ANOVA followed by Dunn's post hoc test was used to determine the statistical significance of multiple groups. *P < 0.05 versus control. Representative fluorescent microscopy images showing the oxidized lipids levels in HIV-1 Tat exposed mPMs, magnification: 20× and scale bar: 10 μm (D). Lipidomics analysis (heatmap; N = 3) showing the altered expression of major phospholipids in HIV-1 Tat exposed microglial cells (E). Bar graph showing the oxidized phosphatidylethanolamine (OxPE) normalized with μg of protein (F). An unpaired Student t-test was used to determine the statistical significance. *P < 0.05 versus control. E– Erastin (5 μM; 48 h), HT-Heat inactivated HIV-1 Tat (100 ng/ml; 48 h).

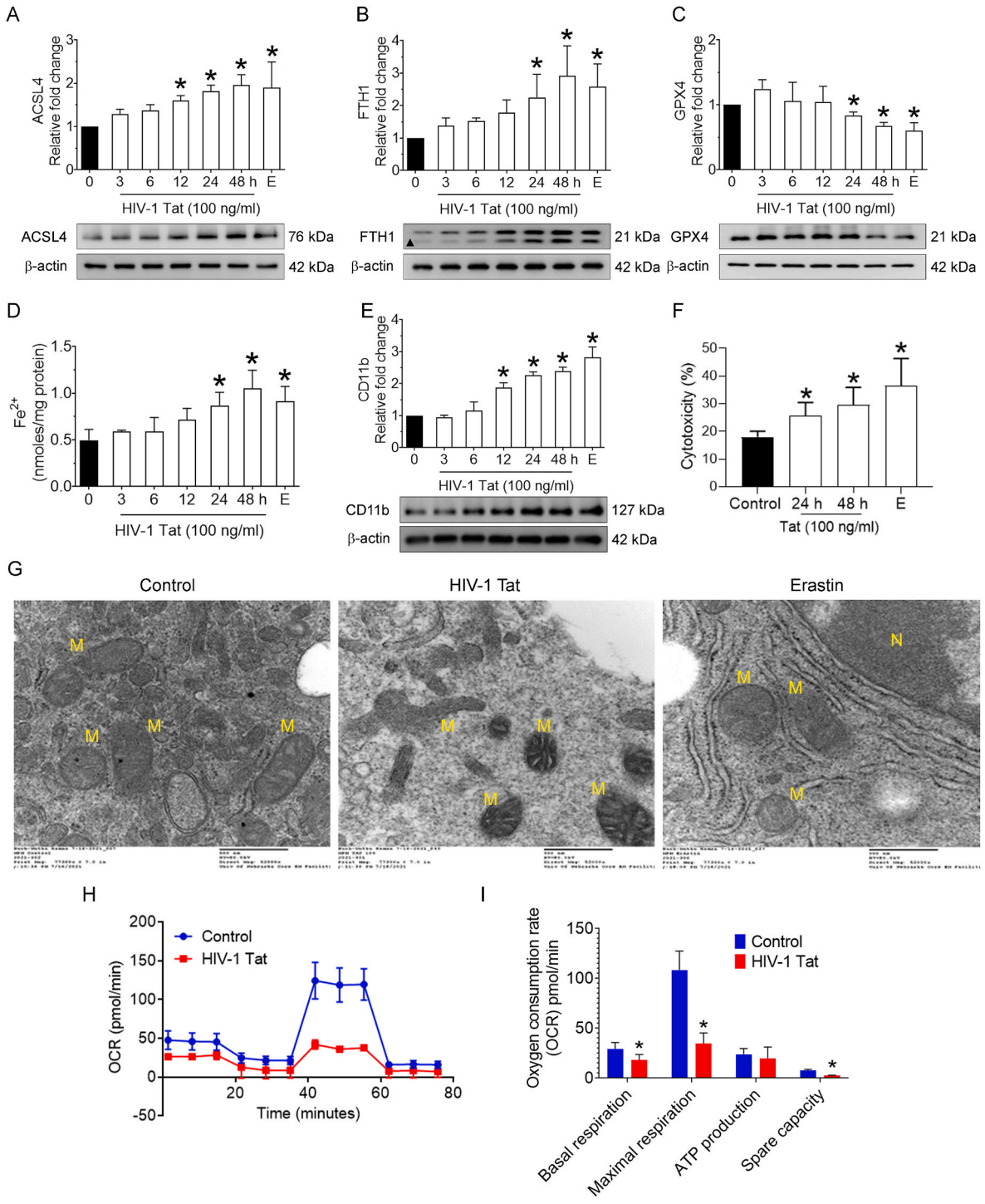

Fig. 2. HIV-1 Tat-mediated induction of ferroptosis in mPMs.
Representative western blotting imaging showing the time-dependent expression levels of ACSL4 (A), FTH (B), and GPX4 (C) in HIV-1 Tat (100 ng/ml) exposed mPMs. Bar graph showing the levels of LIP in HIV-1 Tat exposed mPMs in a time-dependent manner (D). Representative western blotting imaging showing the time-dependent expression of CD11b (E) in HIV-1 Tat exposed mPMs. β-actin was used as an internal control for all the experiments. Bar graph showing the levels of cytotoxicity in HIV-1 Tat exposed mPMs (F). The data are presented as mean ± SD from 6 independent experiments. Nonparametric Kruskal–Wallis one-way ANOVA followed by Dunn's post hoc test was used to determine the statistical significance of multiple groups. *P < 0.05 versus control. Representative Transmission electron microscopic images showing the altered mitochondrial ultrastructure in HIV-1 Tat exposed mPMs (G). N, nucleus; M, mitochondria. Scale bar: 500 nm. Seahorse mitostress analysis showing the OCR levels in HIV-1 Tat exposed mPMs (H). Bar graph showing individual mitochondrial function parameters calculated from the OCR data (I). The data are presented as mean ± SD from 3 independent experiments. Nonparametric Kruskal–Wallis one-way ANOVA followed by Dunn's post hoc test was used to determine the statistical significance of multiple groups. *P < 0.05 versus control; #P < 0.05 versus HIV-1 Tat. E− Erastin (5 μM; 48 h).

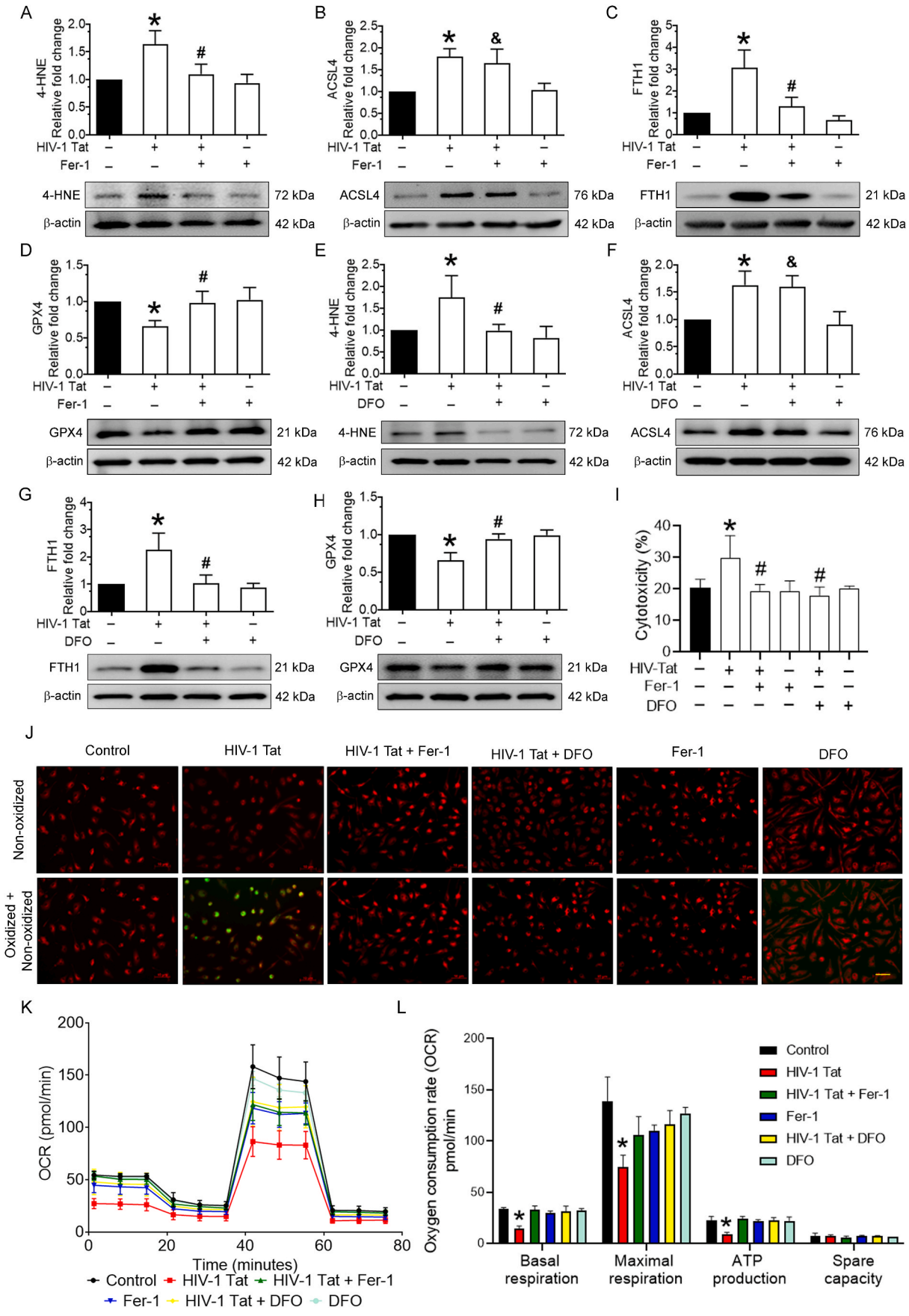

(caption on next page)

Fig. 3. Pharmacological inhibition of ferroptosis in HIV-1 Tat-exposed mPMs.
Representative western blotting imaging showing the expression levels of 4-HNE (A), ACSL4 (B), FTH (C), and GPX4 (D) in Fer-1 (10 μM; 1 h) pretreated and HIV-1 Tat (100 ng/ml) exposed mPMs. Representative western blotting imaging showing the expression levels of 4-HNE (E), ACSL4 (F), FTH (G), and GPX4 (H) in DFO (2 μM; 1 h) pretreated and HIV-1 Tat (100 ng/ml) exposed mPMs. β-actin was used as an internal control for all the experiments. The data are presented as mean ± SD from 6 independent experiments. Nonparametric Kruskal–Wallis one-way ANOVA followed by Dunn's post hoc test was used to determine the statistical significance of multiple groups. *$P < 0.05$ versus control; $^{\#}P < 0.05$ versus HIV-1 Tat; $^{\&}$Not significant versus HIV-1 Tat. Bar graph showing the cytotoxicity in mPMs pretreated with Fer-1 (10 μM; 1 h) or DFO (2 μM; 1 h) followed by HIV-1 Tat (100 ng/ml) for 24 h (I). Representative fluorescent microscopy images showing the oxidized lipids levels in either Fer-1 (10 μM; 1 h) or DFO (2 μM; 1 h) pretreated and HIV-1 Tat (100 ng/ml) exposed mPMs; magnification: 20× and scale bar: 10 μm (J). Seahorse mitostress analysis showing the OCR levels in either Fer-1 (10 μM; 1 h) or DFO (2 μM; 1 h) pretreated and HIV-1 Tat (100 ng/ml) exposed mPMs (K). Bar graph showing individual mitochondrial function parameters calculated from the OCR data (L). The data are presented as mean ± SD from 3 independent experiments. Nonparametric Kruskal–Wallis one-way ANOVA followed by Dunn's post hoc test was used to determine the statistical significance of multiple groups. *$P < 0.05$ versus control; $^{\#}P < 0.05$ versus HIV-1 Tat. Fer-1: Ferrostatin, DFO: Deferoxamine.

protein. For this, mPMs were exposed to varying doses of HIV-1 Tat (25 ng–200 ng/ml) for 48 h, and the levels of 4-HNE adducts were measured by western blotting. As shown in Fig. 1A, the expression of 4-HNE was dose-dependently increased in mPMs with increased expression in cells exposed to 100 ng/ml of HIV-1 Tat compared with control cells. As expected, there was an increased expression of 4-HNE in the erastin (5 μM; 48 h)-exposed mPMs (positive control) and no significant expression in mPMs exposed to heat-inactivated HIV-1 Tat (100 ng/ml). Based on these findings, HIV-1 Tat (100 ng/ml) was selected for all further experiments.

Since exposure of mPMs to HIV-1 Tat increased the levels of 4-HNE in a dose-dependent manner, we next performed a time-course experiment in mPMs exposed to 100 ng/ml of HIV-1 Tat for varying time points (0, 3, 6, 12, 24, and 48 h) and assessed the lysates for the expression of 4-HNE adducts and the formation of MDA. The levels of 4-HNE (Fig. 1B) and MDA (Fig. 1C) were time-dependently increased in mPMs exposed to HIV-1 Tat, with the maximal increase observed at 24 and 48 h. As expected, erastin treatment (5 μM; 48 h) elicited increased levels of 4-HNE (Fig. 1B) and MDA (Fig. 1C) in mPMs. To further confirm the generation of lipid peroxidation products, we measured lipid oxidation using C11-BODIPY™ (581/591) staining, a redox-sensitive dye that integrates into membranes and shifts its fluorescence from red to green upon oxidation. mPMs were exposed to either HIV-1 Tat or erastin for 48 h, followed by incubating the cells with C11-BODIPY™ (581/591) for live imaging. As shown in Fig. 1D, mPMs exposed to HIV-1 Tat and erastin demonstrated increased levels of lipid oxidation compared with control cells. LC-MS Untargeted Lipidomics analysis was also employed to understand HIV-1 Tat-mediated changes in the cellular lipid metabolism in mPMs exposed to HIV-1 Tat (100 ng/ml) for 48 h. As shown in Fig. 1E, LC-MS analysis revealed specific accumulations of different species of phospholipids in HIV-1 Tat exposed mPMs compared with untreated control cells. A significant reduction in phosphatidylethanolamine and phosphatidylcholine was also observed in cells exposed to HIV-1 Tat. In contrast, a significant ($P < 0.05$) increase in oxidized phosphatidylethanolamine was observed in cells exposed to HIV-1 Tat (Fig. 1F). Overall these results strongly suggest that HIV-1 Tat induced lipid oxidation in microglia cells.

3.2. HIV-1 Tat-mediated induction of ferroptosis in mPMs

Next, we sought to determine the consequences of oxidized lipids in mPMs, particularly their role in the execution of iron-dependent cell death, known as ferroptosis. Since ACSL4 plays a crucial role in ferroptosis by producing the ferroptotic precursors, the time-dependent expression of ACSL4 was assessed in mPMs exposed to HIV-1 Tat (100 ng/mL), along with the positive control, erastin (5 μM; 48 h). As shown in Fig. 2A, the expression of ACSL4 was time-dependently increased in HIV-1 Tat-exposed mPMs, and as expected, ACSL4 expression was also significantly ($P < 0.05$) increased in erastin-exposed mPMs. Next, the expression of other ferroptosis markers, such as FTH1 and GPX4, was determined in HIV-1 Tat-exposed mPMs. As expected, and shown in Fig. 2B and C, the expression of FTH1 (Fig. 2B) was time-dependently increased, while that of GPX4 (Fig. 2C) demonstrated a downregulation in HIV-1 exposed mPMs compared with control cells. As expected, mPMs exposed to erastin (5 μM; 48 h) significantly ($p < 0.05$) increased the levels of FTH1 with a concomitant decrease in the levels of GPX4. Cells exposed to heat-inactivated HIV-1 Tat exhibited no significant changes compared with control cells (Fig. 2B and C). Next, we assessed the intracellular levels of LIP in mPMs exposed to HIV-1 Tat (100 ng/ml) for varying times, and as shown in Fig. 2D, the intracellular LIP was significantly ($P < 0.05$) increased in a time-dependent manner in the presence of HIV-1 Tat compared with control cells.

Next, we wanted to determine HIV-1 Tat-mediated microglial activation by determining the expression levels of CD11b. As shown in Fig. 2E, exposure of mPMs to HIV-1 Tat (100 ng/ml) time-dependently increased the expression of CD11b compared with control cells, thus confirming the cellular activation in this experimental setup. We also determined the cellular toxicity in this experimental setup using a lactate dehydrogenase cytotoxicity assay. As expected and shown in Fig. 2F, mPMs exposed to HIV-1 Tat (100 ng/ml) elicited ~20% cell toxicity compared with control cells. Cell toxicity was significantly ($P < 0.05$) increased in erastin-exposed mPMs. We next sought to determine the changes in cellular ultrastructure induced by HIV-1 Tat (100 ng/ml; 48 h) using transmission electron microscopy. There was increased mitochondrial membrane rupture, disruption of cristae, and mitochondrial shrinkage in HIV-1 Tat-exposed mPMs compared with control cells (Fig. 2G). Similar ultrastructural changes were also observed in erastin-exposed mPMs. To further understand the contribution of HIV-1 Tat-mediated microglial ferroptosis, we performed mitochondrial function analysis using the Seahorse XF cell mitostress test in mPMs. As shown in Fig. 2H and I, mPMs exposed to HIV-1 Tat exhibited altered oxygen consumption rate (Fig. 2H) and notable ($P < 0.05$) decrease in mitochondrial basal and maximal respiration, ATP production, and spare respiratory capacity compared with the control mPMs (Fig. 2I). Collectively, these results suggest that HIV-1 Tat induced ferroptosis, as all the hallmarks of ferroptosis were observed in mPMs.

3.3. Pharmacological inhibition of ferroptosis in HIV-1 Tat-exposed mPMs

We next sought to investigate the direct involvement of HIV-1 Tat-mediated ferroptosis in mPMs. For this, we confirmed HIV-1 Tat-mediated ferroptosis using pharmacological inhibitors such as Fer-1 or DFO. For this, mPMs were pretreated with 10 μM Fer-1 or 2 μM DFO for 1 h, followed by exposure with HIV-1 Tat (100 ng/ml; 48 h) and studied for ferroptosis markers such as 4-HNE, ACSL4, FTH1, and GPX4. As shown in Fig. 3A-D, in mPMs exposed to HIV-1 Tat, 4-HNE (Fig. 3A), ACSL4 (Fig. 3B), and FTH1 (Fig. 3C) expressions were significantly ($P < 0.05$) increased with a concomitant decrease in GPX4 (Fig. 3D) expression. In contrast, pretreatment of mPMs with Fer-1 significantly blocked all the key ferroptosis markers except ACSL4 (Fig. 3B). Similar results were found in mPMs pretreated with DFO followed by HIV-1 Tat (100 ng/ml; 48 h) exposure (Fig. 3E-H). Cell toxicity findings also demonstrated that pretreatment of mPMs with either Fer-1 or DFO significantly ($P < 0.05$) ameliorated cellular cytotoxicity induced by HIV-1 Tat (Fig. 3I). Next, we determined lipid oxidation levels using C11-BODIPY™ (581/591)

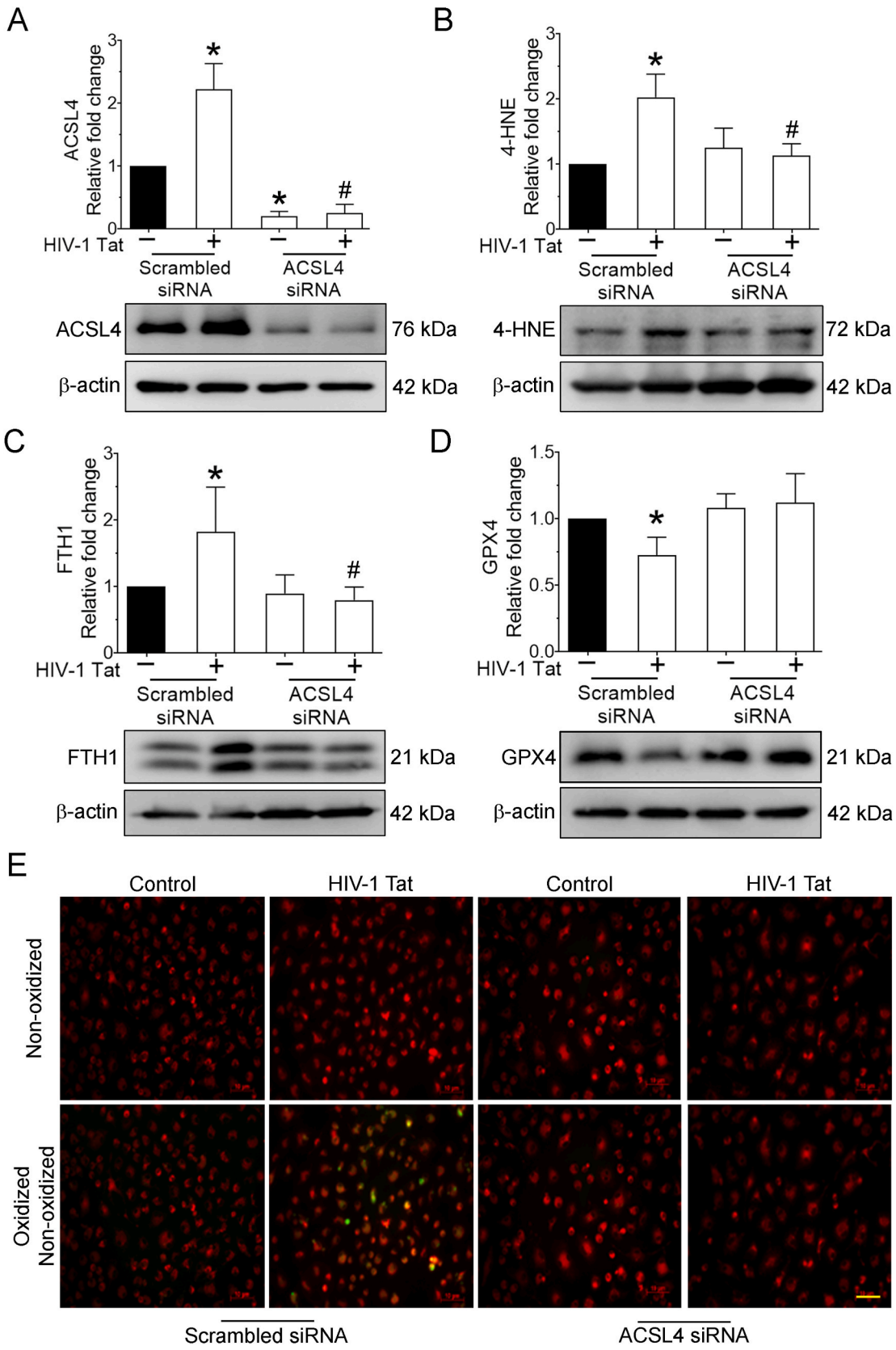

Fig. 4. HIV-1 Tat-mediated induction of ferroptosis involved ACSL4 in mPMs.
Representative western blotting imaging showing the expression levels of 4-HNE (A), ACSL4 (B), FTH (C), and GPX4 (D) in ACSL4 silenced mPMs exposed with HIV-1 Tat (100 ng/ml; 48 h). β-actin was used as an internal control for all the experiments. The data are presented as mean ± SD from 6 independent experiments. Nonparametric Kruskal–Wallis one-way ANOVA followed by Dunn's post hoc test was used to determine the statistical significance of multiple groups. *$P < 0.05$ versus control; $^{\#}P < 0.05$ versus HIV-1 Tat. Representative fluorescent microscopy images showing the oxidized lipids levels in ACSL4 silenced mPMs exposed with HIV-1 Tat, magnification: 20× and scale bar: 10 μm (E).

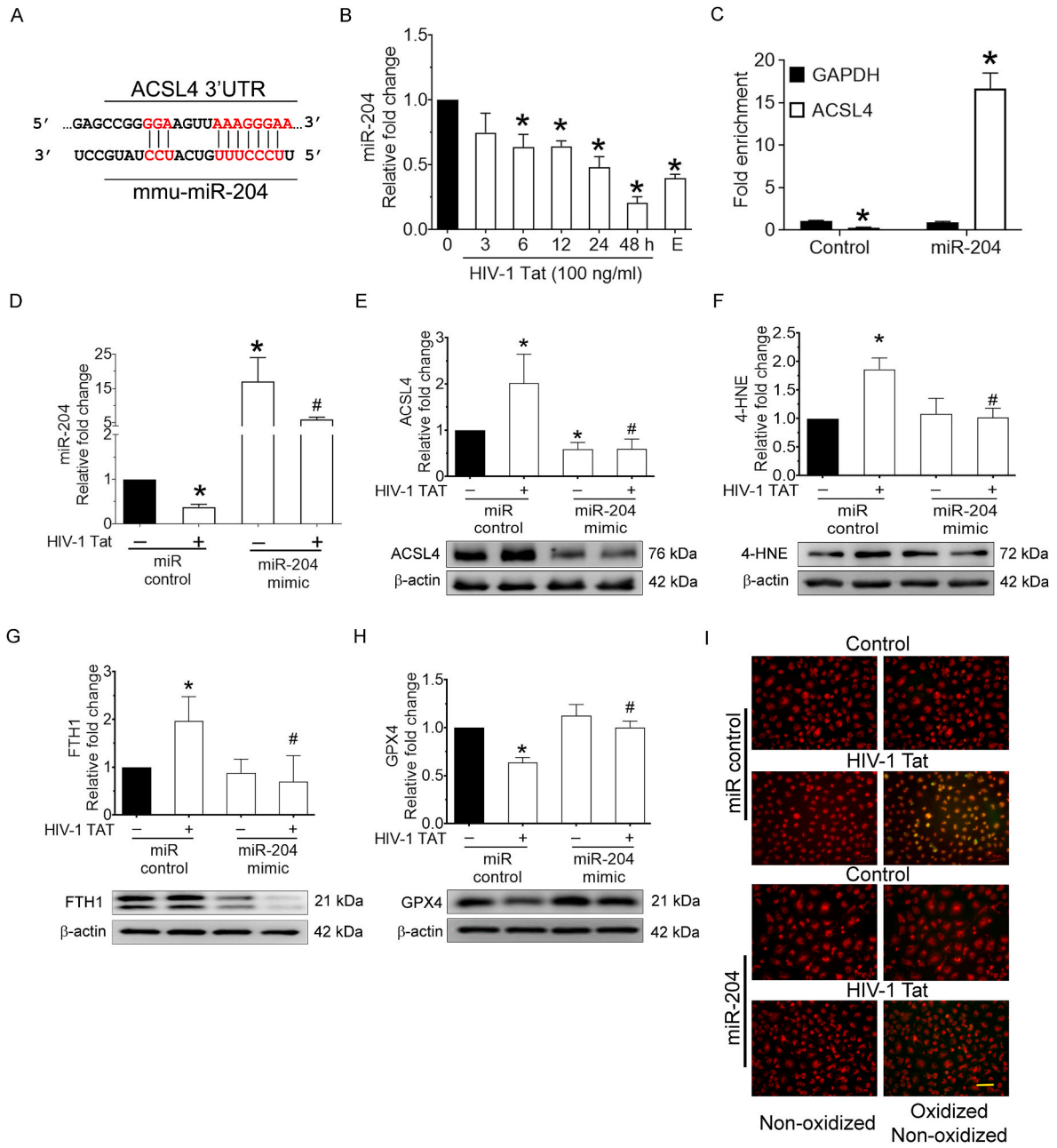

Fig. 5. miR-204 targets 3′-UTR of ACSL4 in mPMs.
The putative binding site of miR-204 in the 3′-UTR of mouse ACSL4 mRNA (A). The potential complementary binding residues are shown in red color. Representative qPCR analysis showing time-dependent downregulation of miR-204 expression in HIV-1 Tat (100 ng/ml; 48 h) exposed mPMs (B). U6 was used as an endogenous control. miRNA target validation assay confirmed increased enrichment of ACSL4, the miR-204 target mRNA, in miR-204 overexpressed BV2 cells. GAPDH was used as an endogenous control (C). Representative qPCR analysis showing the transfection efficiency of miR-204 in mPMs overexpressed with miR-204 mimic followed by HIV-1 Tat (100 ng/ml; 48 h) exposure (D). U6 was used as an endogenous control. Representative western blotting imaging showing the expression levels of ACSL4 (E), 4-HNE (F), FTH (G), and GPX4 (H) in mPMs overexpressed with miR-204 mimic followed by HIV-1 Tat (100 ng/ml; 48 h) exposure. β-actin was used as an internal control for all the experiments. The data are presented as mean ± SD from 6 independent experiments. Nonparametric Kruskal–Wallis one-way ANOVA followed by Dunn's post hoc test was used to determine the statistical significance of multiple groups. *P < 0.05 versus control; #P < 0.05 versus HIV-1 Tat. Representative fluorescent microscopy images showing the oxidized lipids levels in mPMs overexpressed with miR-204 mimic followed by HIV-1 Tat (100 ng/ml; 48 h) exposure, magnification: 20× and scale bar: 10 μm (I). (For interpretation of the references to color in this figure legend, the reader is referred to the Web version of this article.)

staining and found that HIV-1 Tat-mediated increased lipid oxidation was notably blocked in mPMs pretreated with both Fer-1 and DFO followed by HIV-1 Tat exposure (Fig. 3J). Next, we assessed mitochondrial functional analysis in mPMs pretreated with either Fer-1 or DFO followed by HIV-1 Tat exposure for 48 h. As shown in Fig. 3K and L, mitochondrial respiration (basal and maximal respiration and ATP production) was significantly ($P < 0.05$) increased in the presence of both Fer-1 and DFO in HIV-1 Tat exposed mPMs compared with control cells. Together, these findings indicate that HIV-1 Tat directly induced ferroptosis in mPMs, and both Fer-1 and DFO did not reverse the levels of ACSL4, suggesting that ACSL4 could be an upstream signaling mediator.

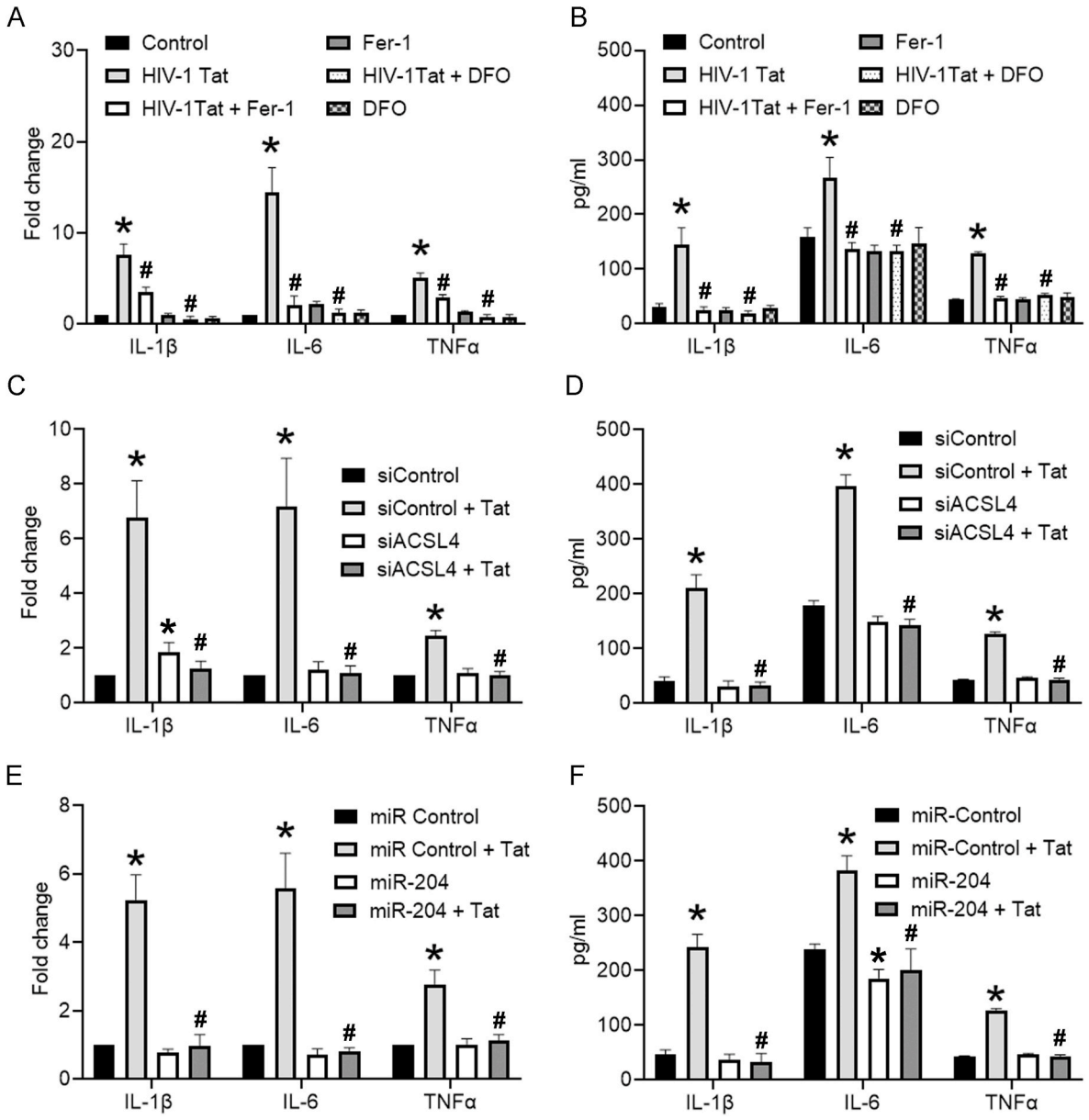

Fig. 6. HIV-1 Tat-mediated ferroptosis induced proinflammatory cytokines in mPMs.
qPCR (A) and ELISA (B) analysis showing the expression levels of proinflammatory cytokines such as IL1β, IL6, and TNFα in either Fer-1 (10 μM; 1 h) or DFO (2 μM; 1 h) pretreated and HIV-1 Tat (100 ng/ml) exposed mPMs. qPCR (C) and ELISA (D) analysis showing the expression levels of proinflammatory cytokines such as IL1β, IL6, and TNFα in ACSL4 silenced mPMs exposed with HIV-1 Tat (100 ng/ml; 48 h). qPCR (E) and ELISA (F) analysis showing the expression levels of proinflammatory cytokines such as IL1β, IL6, and TNFα in mPMs overexpressed with miR-204 mimic followed by HIV-1 Tat (100 ng/ml; 48 h) exposure. The data are presented as mean ± SD from 6 independent experiments. Nonparametric Kruskal–Wallis one-way ANOVA followed by Dunn's post hoc test was used to determine the statistical significance of multiple groups. *$P < 0.05$ versus control; #$P < 0.05$ versus HIV-1 Tat.

3.4. HIV-1 Tat-mediated induction of ferroptosis involved ACSL4 in mPMs

To further understand whether ACSL4 was an upstream mediator in HIV-1 Tat-mediated ferroptosis in mPMs, we employed the gene silencing approach using ACSL4 siRNA. mPMs were transfected with either scrambled or mouse-specific ACSL4 siRNA followed by HIV-1 Tat (100 ng/ml; 48 h) exposure. As shown in Fig. 4A, there was efficient inhibition of ACSL4 expression in ACSL4 siRNA transfected cells compared with control cells. We next determined the expression levels of 4-HNE, FTH1, GPX4, and lipid oxidation in ACSL4 silenced, HIV-1 Tat, exposed mPMs. ACSL4 siRNA silenced mPMs failed to induce HIV-1 Tat-mediated ferroptosis markers such as 4-HNE (Fig. 4B), FTH1 (Fig. 4C), GPX4 (Fig. 4D), and lipid oxidation (Fig. 4E). Together, these findings suggest that ACSL4 silencing inhibited or reversed HIV-1 Tat-mediated ferroptosis. Hence, we hypothesize that ACSL4 is upstream of HIV-1 Tat-mediated ferroptosis.

3.5. miR-204 targets 3′-UTR of ACSL4 in mPMs

Our results thus far are consistent with a model that ACSL4 could be an upstream in HIV-1 Tat mediated ferroptosis in mPMs. We next sought to explore the upstream modulator for ACSL4 expression. Based on the TargetScan analysis, ACSL4 is a predicted novel target of miR-204 and has a highly conserved 3′-untranslated region (UTR) binding site for miR-204 (Fig. 5A). We thus next sought to determine time-dependent expression levels of miR-204 in HIV-1 Tat (100 ng/ml) exposed mPMs. As shown in Fig. 5B, the expression of miR-204 was time-dependently

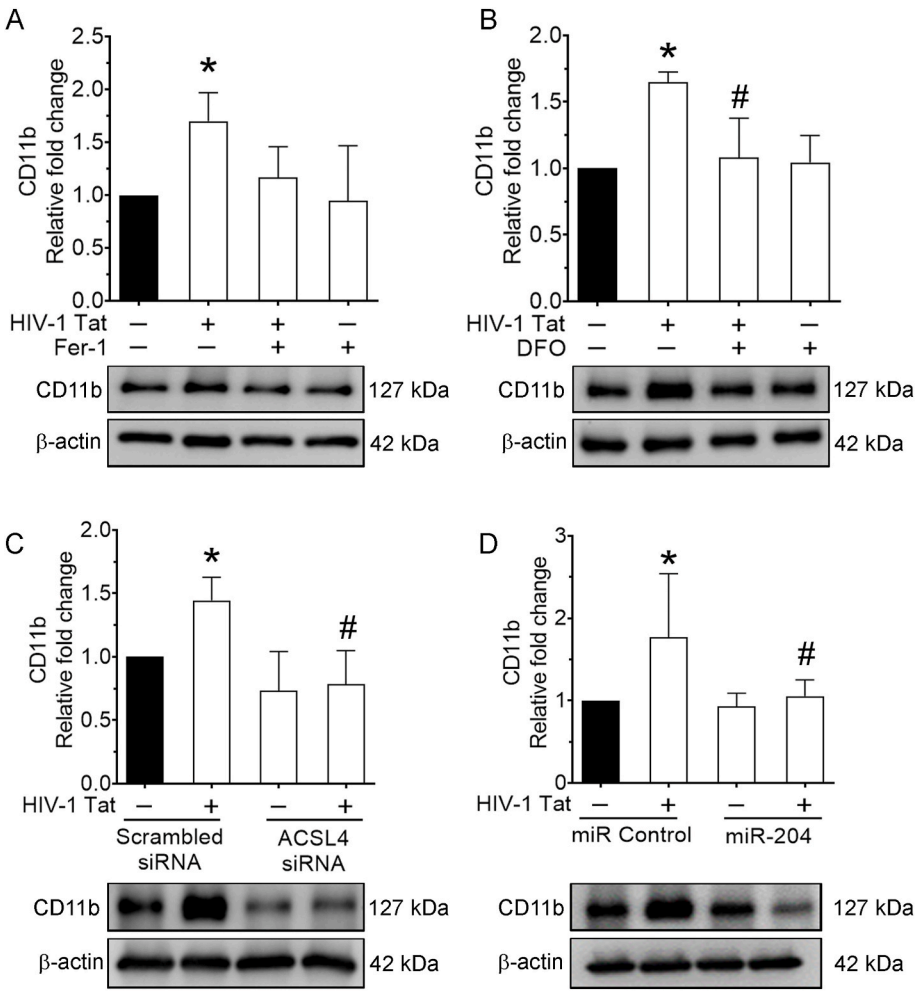

Fig. 7. HIV-1 Tat-mediated ferroptosis induced cellular activation in mPMs.
Representative western blotting imaging showing the expression levels of CD11b in either Fer-1 (10 μM; 1 h) or DFO (2 μM; 1 h) pretreated and HIV-1 Tat (100 ng/ml) exposed mPMs (A and B). Representative western blotting imaging showing the expression levels of CD11b in ACSL4 silenced mPMs exposed with HIV-1 Tat (C). Representative western blotting imaging showing the expression levels of CD11b in mPMs overexpressed with miR-204 mimic followed by HIV-1 Tat (D) exposure. β-actin was used as an internal control for all the experiments. The data are presented as mean ± SD from 6 independent experiments. Nonparametric Kruskal–Wallis one-way ANOVA followed by Dunn's post hoc test was used to determine the statistical significance of multiple groups. *P < 0.05 versus control; #P < 0.05 versus HIV-1 Tat.

decreased in mPMs exposed to HIV-1 Tat, and as expected, erastin-treated mPMs also elicited downregulation of miR-204. To further confirm the direct binding and regulation of miR-204 with the 3′-UTR of ACSL4, we performed argonaute immunoprecipitation using a miR target validation kit per the manufacturer's instructions. As shown in Fig. 5C, miR Target IP confirmed ACSL4 as a direct target of miR-204, based on significant ($P < 0.05$) enrichment of ACSL4 mRNA bound to Ago protein in cells overexpressing miR-204 mimic.

Next, we wanted to demonstrate the role of miR-204 in HIV-1 Tat-mediated ferroptosis in mPMs. mPMs were transfected with either miR-control or miR-204 mimic, followed by HIV-1 Tat (100 ng/ml; 48 h) exposure for determining the expression of miR-204, ACSL4, 4-HNE, FTH1, GPX4 and lipid oxidation. We first determined the transfection efficiency of miR-204 in miR-204 mimic transfected, HIV-1 Tat exposed mPMs using qPCR (Fig. 5D). As shown in Fig. 5E-I, HIV-1 Tat-mediated increased expression of ACSL4 (Fig. 5E), 4-HNE (Fig. 5F), FTH1 (Fig. 5G), and lipid oxidation (Fig. 5I) with a concomitantly decreased expression of GPX4 (Fig. 5H), and this was significantly ($P < 0.05$) reversed in miR-204 overexpressed mPMs exposed to HIV-1 Tat. These results suggest that miR-204 is upstream of ACSL4, and overexpression of miR-204 mimic reduced HIV-1 Tat-mediated ferroptosis in mPMs.

3.6. HIV-1 Tat-mediated ferroptosis induced proinflammatory cytokines in mPMs

We next sought to determine the interplay of ferroptosis and the release of proinflammatory cytokines in HIV-1 Tat-exposed mPMs. mPMs were pretreated with either Fer-1 (10 μM; 1 h) or DFO (2 μM; 1 h), followed by HIV-1 Tat (100 ng/ml; 48 h) exposure and assessed for the production of proinflammatory cytokines such as interleukin (IL)1β, IL6, and tumor necrosis factor (TNF)-α using both qPCR and ELISA. As shown in Fig. 6A and B, inhibition of ferroptosis by Fer-1 or DFO significantly ($P < 0.05$) inhibited HIV-1 Tat-mediated increased mRNA (Fig. 6A) and protein (Fig. 6B) expression of IL1β, IL6, and TNFα in mPMs. Similarly, gene silencing of ACSL4 (Fig. 6C and D) and overexpression of miR-204 (Fig. 6E and F) also significantly ($P < 0.05$) reduced HIV-1 Tat-mediated increased expression proinflammatory cytokines (IL1β, IL6, and TNFα). These results suggest that inhibition of ferroptosis reduced the HIV-1 Tat mediated inflammation.

3.7. HIV-1 Tat-mediated ferroptosis induced cellular activation in mPMs

Since, we found that inhibition of ferroptosis reduced the levels of inflammation. Next, we sought to determine the cellular activation status in the context of HIV-1 Tat-meditated ferroptosis in mPMs. mPMs were pretreated with either Fer-1 (10 μM) or DFO (2 μM) for 1 h, followed by exposure of cells to HIV-1 Tat (100 ng/ml; 48 h) and lysates were used to determine the expression of microglial activation marker, CD11b. As shown in Fig. 7A and B, inhibition of ferroptosis by pre-treatment of mPMs with Fer-1 or DFO followed by HIV-1 Tat exposure ameliorated HIV-1 Tat-mediated induction of CD11b (cellular activation) expression. Similarly, gene silencing of ACSL4 (Fig. 7C) and overexpression of miR-204 (Fig. 7D) also significantly ($P < 0.05$) reduced HIV-1 Tat-mediated increased microglial activation in mPMs. Consistent with the results for pro-inflammatory cytokines, inhibition of ferroptosis reduced the levels of microglia activation mediated by HIV-1

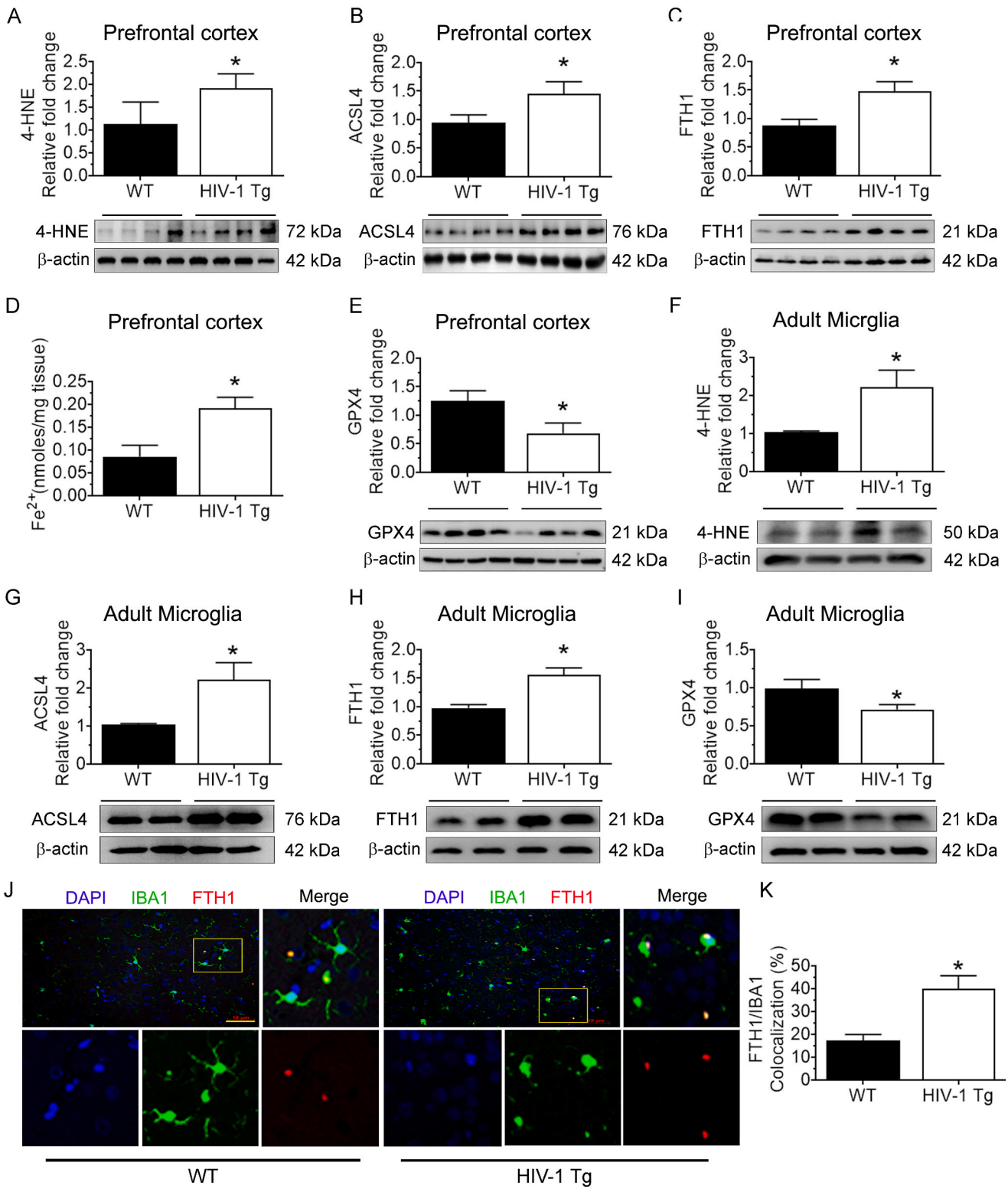

Fig. 8. Microglial ferroptosis in the brains of HIV-1 Tg rats.
Representative western blotting imaging showing the ferroptosis markers such as 4-HNE (A), ACSL4 (B), FTH1 (C), LIP (D), and GPX4 (E) in the frontal cortices of wild-type and HIV-1 Tg rats (n = 4). β -actin was probed as a protein loading control for all experiments. Representative western blotting imaging showing the ferroptosis markers such as 4-HNE (F), ACSL4 (G), FTH1 (H), and GPX4 (I) in the adult microglia isolated from the cortices of wild-type and HIV-1 Tg rats (n = 4). Representative immunofluorescence staining for IBA1, microglial activation marker (green), FTH1 (red), and DAPI (blue) in the frontal cortices of wild-type and HIV-1 Tg rats, magnification: 20× and scale bar: 10 μm (J). Bar graph showing the percentage colocalization of FTH1 with IBA-1 in the frontal cortices of wild-type and HIV-1 Tg rats. β-actin was probed as a protein loading control for all experiments. An unpaired Student t-test was used to determine the statistical significance. *P < 0.05 versus control. (For interpretation of the references to color in this figure legend, the reader is referred to the Web version of this article.)

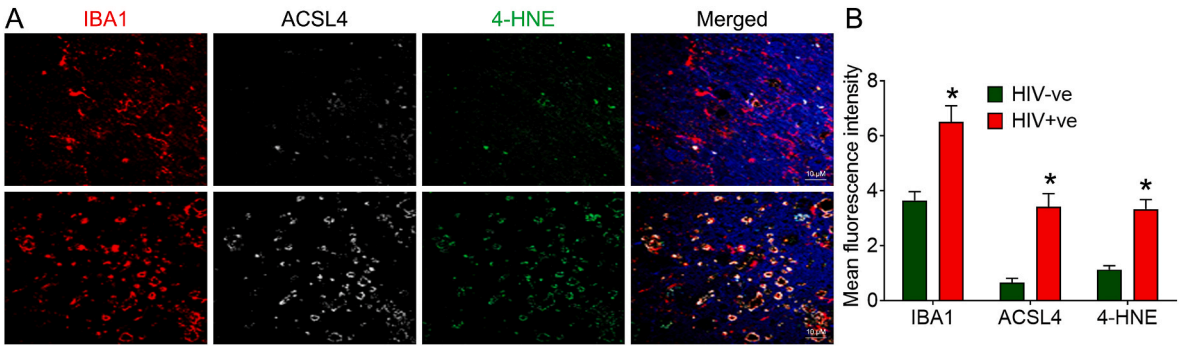

Fig. 9. Increased expression of ferroptosis markers in the brains of HIV + ve individuals.
Representative immunofluorescence staining for IBA1, microglial activation marker (red), ACSL4 (white), 4-HNE (green), and DAPI (blue) in the frontal cortices of HIV-ve and HIV + ve individuals, magnification: 100× and scale bar: 10 μm (A). Bar graph showing the mean fluorescence intensity of ferroptosis markers such as ASCL4 and 4-HNE in the frontal cortices of HIV-ve and HIV + ve individuals. An unpaired Student t-test was used to determine the statistical significance. *P < 0.05 versus HIV-ve. (For interpretation of the references to color in this figure legend, the reader is referred to the Web version of this article.)

Tat.

3.8. Microglial ferroptosis in the brains of HIV-1 Tg rats

We next sought to validate the *in vitro* findings in the brains of HIV-1 Tg rats *in vivo*. 15-month-old male HIV-1 Tg rats and their corresponding wild-type rats were used in this study. As shown in Fig. 8A-E, the expression of 4-HNE (Fig. 8A), ACSL4 (Fig. 8B), FTH1 (Fig. 8C), and the levels of LIP (Fig. 8D) were significantly ($P < 0.05$) increased in the frontal cortices of HIV-1 Tg rats compared with wild type controls. Similar to the *in vitro* findings, we also found a concomitant decrease in the expression of GPX4 (Fig. 8E) in the brains of these rats. Similar results were found in the other brain regions, such as the striatum (Fig. S1) and hippocampus (Fig. S2) of HIV-1 Tg rats, compared with the same regions of wild-type controls. However, the levels of GPX4 were not significantly ($P < 0.05$) reduced in the hippocampus (Fig. S2). We also performed *ex vivo* adult microglia isolation from the frontal cortices of HIV-1 Tg rats and assessed them for the expression of ferroptosis markers. As shown in Fig. 8F-I, all the ferroptosis markers, such as 4-HNE (Fig. 8F), ACSL4 (Fig. 8G), and FTH1 (Fig. 8H), were increased. At the same time, the expression of GPX4 was decreased (Fig. 8I) in *ex vivo* adult microglia isolated from the frontal cortices of HIV Tg rats compared with adult microglia from the same region of wild-type rats. Immunofluorescence for the microglial-specific expression of FTH1 was also performed in the frontal cortices of HIV-1 Tg and wild-type rats. As shown in Fig. 8J, we found increased intensity and localization of FTH1 with Iba1 in the frontal cortices of HIV-1 Tg rats versus wild-type rats. These results validated our *in vitro* findings, and further confirmed the induction of ferroptosis in the context of HIV.

3.9. Increased expression of ferroptosis markers in the brains of HIV + ve individuals

We next validated our findings in the frontal cortices of HIV + ve individuals. For this, we assessed the localization and expression levels of key ferroptosis markers, ACSL4 and 4-HNE, in the frontal cortices of HIV + ve individuals and their age-matched negative controls. As shown in Fig. 9A and B, the mean fluorescence intensity of ACSL4 and 4-HNE was high in HIV + ve individuals compared to their controls. All the HIV + ve individuals were on cART at the time of death. Overall, this study confirmed the involvement of ferroptosis in HIV-1/HIV-1 Tat-mediated microglial activation.

4. Discussion

Microglia have been identified as critical players in tissue homeostasis and disease pathogenesis and are highly reactive cells that respond to aberrations such as increased iron levels. Of the various CNS cells containing iron, microglia are the most iron-rich cells [78]. These cells have been implicated as the guardians of ferroptosis within the neuronal system owing to their critical role in brain diseases involving iron accumulation [78,79]. While many studies implicating HIV-1 Tat-mediated induction of lipid peroxidation products in microglia are extant [80–82], the concept of HIV-1 Tat-mediated ferroptosis in microglial cells largely remains unexplored. This study, for the first time, underscores the detrimental effects of HIV-1 Tat on the induction of ferroptosis in microglial cells with the involvement of the miR-204–ACSL4 axis.

ACSL4 catalyzes the activation of fatty acids by introducing CoA and then incorporating it into phospholipids. In a milieu of rich oxidant products, these phospholipids are the primary target for lipid oxidation [83,84]. Recent studies have reported high expression of ACSL4-induced ferroptosis in many cell types, including microglia [85–87]. These findings show that increased ACSL4 plays a vital role in ferroptosis execution. We demonstrated increased lipid oxidation products in microglial cells exposed to HIV-1 Tat.

Lipid peroxidation is a hallmark of ferroptosis and directly abolishes cellular membranes, thereby causing ferroptosis [83]. It has been shown that ferroptosis inhibitors, such as Fer-1 (a synthetic antioxidant) or DFO (an iron chelating agent), inhibited graphene quantum dots-mediated ferroptosis in microglial cells [56]. Along these lines, we also used Fer-1 and DFO inhibitors in this study and confirmed HIV-1 Tat-mediated ferroptosis in microglial cells, suggesting that HIV-1 Tat-induced ferroptosis involved increased lipid peroxidation and iron levels in microglial cells. Emerging studies have revealed a direct link between low levels of reduced glutathione that directly impacts GPX4 activity [88] and impaired survival in HIV-1 infection [89] and increased production of lipid peroxidation in PLWH [39,90–93]. It has also been demonstrated that GPX4 deficiency increases lipid oxidation, resulting in the generation of various lipid peroxidation products and, ultimately, cell death [38]. GPX4 is critical for repairing oxidized lipids to prevent ferroptosis. In this study, we demonstrated that HIV-1 Tat exposure downregulated the expression levels of GPX4 in mPMs.

Further, ferroptosis is linked with mitochondrial damage, bioenergetics, and metabolism in various disease conditions [94,95]. In this study, HIV-1 Tat altered mitochondrial ultrastructure and mitochondrial respiration in microglial cells. Inhibition of ferroptosis improved mitochondrial respiration, thus suggesting mitochondrial involvement in this process. In addition, we also found that silencing of ACSL4 in mPMs ameliorated microglial activation and suppressed the secretion of proinflammatory cytokines in mPMs exposed to HIV-1 Tat. Similarly, Fer-1 or DFO pretreatment also notably reduced the production of the proinflammatory cytokines in HIV-1 Tat-exposed mPMs. The relationship between lipid peroxidation and proinflammatory cytokine

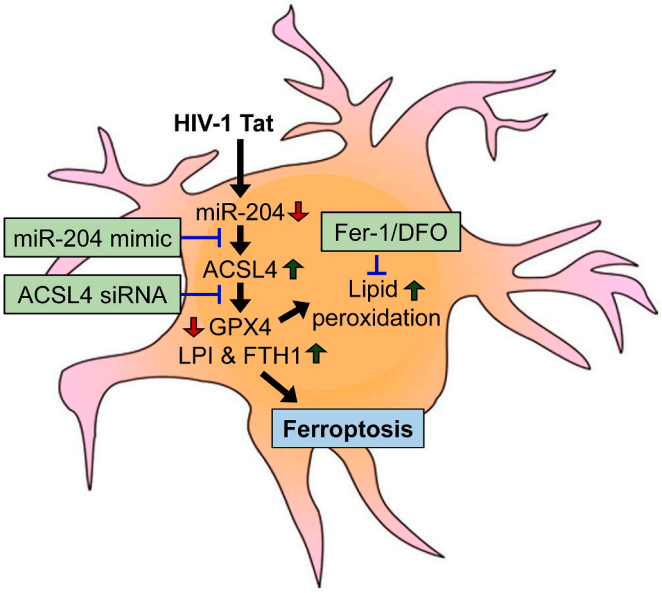

Fig. 10. Schematic showing the proposed mechanism involved in HIV-1 Tat-mediated microglial ferroptosis.

secretion is well-established in microglia during neuroinflammation [96,97]. We validated the *in vitro* findings in a well-established animal model, HIV-1 Tg rats.

For the current study, we chose the HIV-1 Tg rats [98]. These rats serve as a suitable model for NeuroHIV mimicking PLWH on cART [99–102]. As expected, our *in vivo* studies also found increased expression of 4-HNE, ACSL4, FTH1, and lipid peroxidation and decreased expression of GPX4 in the prefrontal cortex of these animals as well as *ex vivo* isolated adult microglia of HIV-1 Tg rats compared with the wild-type controls. Similar to HIV-1 Tg rats, HIV + ve human frontal cortex brain samples also showed higher expression of ACSL4 and 4-HNE with IBA1+ve microglia, demonstrating the prevalence of ferroptosis in HIV + ve human frontal cortex brain samples.

It is well-known that CNS homeostasis involves crosstalk among various CNS cells, including microglia and neurons. These interactions range from direct cell-to-cell contact to the use of soluble factors for short and long-distance biological material transfer across cells. Both vesicular and non-vesicular mechanisms mediate these interactions [103]. Several growth factors, neurotransmitters, proinflammatory cytokines, chemokines, innate-immune mediators, tissue damage molecules, ROS, and metabolic mediators like glutamate are exchanged through these interactions among microglia, astrocytes, and neurons [104,105]. Emerging studies also point out that microglia-released extracellular vesicles (EVs) are used to communicate with astrocytes and neurons since these EVs contain active biomolecules such as mRNA, proteins, and non-coding RNAs that can modulate the expression of target genes in the recipient cells. More recently, findings from our lab have reported that EVs released from HIV-1 Tat exposed microglia carry microglial enriched inflammasome protein, NLRP3, and the proinflammatory cytokine, IL1β that can be taken up by the neurons, leading to somatodendritic injury [106]. Likely, HIV-1 Tat-mediated microglial ferroptosis could also involve the transfer of oxidized lipids, LIP, and lipid peroxidation products to neighboring glial cells such as astrocytes and neurons. Collectively, ferroptosis could thus contribute to the neuroinflammatory milieu underlying the pathogenesis of NeuroHIV. Studies also demonstrated an increased accumulation of ferritin heavy chain in the cortices of HIV-1 Tg rats, and the accumulation of ferritin heavy chain was speculated with the HIV-1 viral protein, gp120 via TNFα and IL1β signaling [68].

In summary, this study confirmed that HIV-1 Tat-induced microglial ferroptosis by downregulating the expression of miR-204, which, in turn, upregulated the expression of its target - ACSL4. Increased expression of ACSL4 resulted in increased lipid peroxidation leading to microglial activation and secretion of pro-inflammatory cytokines, eventually resulting in neuroinflammation (Fig. 10). Blocking of ACSL4-dependent microglial ferroptosis could thus be considered a potential therapeutic target for ameliorating neuroinflammation associated with HAND. However, further studies are needed to understand the molecular mechanism(s) underlying ACSL4-mediated ferroptosis in HIV-1 Tat-mediated microglial activation and its functions.

Declaration of competing interest

The authors declare that they have no known competing financial interests or personal relationships that could have appeared to influence the work reported in this paper.

Data availability

Data will be made available on request.

Acknowledgments

This work was funded by the National Institutes of Health - National Institute on Drug Abuse: DA044586 (S B), DA047156 (S B), DA050545 (S B), and DA052266 (P P). The support from Nebraska Center for Substance Abuse Research (NCSAR) is also highly acknowledged.

Appendix A. Supplementary data

Supplementary data to this article can be found online at https://doi.org/10.1016/j.redox.2023.102689.

References

[1] M. Weichseldorfer, M. Reitz, O.S. Latinovic, Past HIV-1 medications and the current status of combined antiretroviral therapy options for HIV-1 patients, Pharmaceutics 13 (2021).
[2] A. Nath, K. Psooy, C. Martin, B. Knudsen, D.S. Magnuson, N. Haughey, J. D. Geiger, Identification of a human immunodeficiency virus type 1 Tat epitope that is neuroexcitatory and neurotoxic, J. Virol. 70 (1996) 1475–1480.
[3] S. Fitting, R. Xu, C. Bull, S.K. Buch, N. El-Hage, A. Nath, P.E. Knapp, K.F. Hauser, Interactive comorbidity between opioid drug abuse and HIV-1 Tat: chronic exposure augments spine loss and sublethal dendritic pathology in striatal neurons, Am. J. Pathol. 177 (2010) 1397–1410.
[4] N.J. Hargus, S.A. Thayer, Human immunodeficiency virus-1 Tat protein increases the number of inhibitory synapses between hippocampal neurons in culture, J. Neurosci. 33 (2013) 17908–17920.
[5] H.J. Kim, K.A. Martemyanov, S.A. Thayer, Human immunodeficiency virus protein Tat induces synapse loss via a reversible process that is distinct from cell death, J. Neurosci. 28 (2008) 12604–12613.
[6] I. Mocchetti, A. Bachis, V. Avdoshina, Neurotoxicity of human immunodeficiency virus-1: viral proteins and axonal transport, Neurotox. Res. 21 (2012) 79–89.
[7] A.H. Shin, S.A. Thayer, Human immunodeficiency virus-1 protein Tat induces excitotoxic loss of presynaptic terminals in hippocampal cultures, Mol. Cell. Neurosci. 54 (2013) 22–29.
[8] S.L. Wesselingh, C. Power, J.D. Glass, W.R. Tyor, J.C. McArthur, J.M. Farber, J. W. Griffin, D.E. Griffin, Intracerebral cytokine messenger RNA expression in acquired immunodeficiency syndrome dementia, Ann. Neurol. 33 (1993) 576–582.
[9] M.O. Westendorp, R. Frank, C. Ochsenbauer, K. Stricker, J. Dhein, H. Walczak, K. M. Debatin, P.H. Krammer, Sensitization of T cells to CD95-mediated apoptosis by HIV-1 Tat and gp120, Nature 375 (1995) 497–500.
[10] H.C. Chang, F. Samaniego, B.C. Nair, L. Buonaguro, B. Ensoli, HIV-1 Tat protein exits from cells via a leaderless secretory pathway and binds to extracellular matrix-associated heparan sulfate proteoglycans through its basic region, AIDS 11 (1997) 1421–1431.
[11] M. Tyagi, M. Rusnati, M. Presta, M. Giacca, Internalization of HIV-1 tat requires cell surface heparan sulfate proteoglycans, J. Biol. Chem. 276 (2001) 3254–3261.
[12] I.E. Andras, H. Pu, M.A. Deli, A. Nath, B. Hennig, M. Toborek, HIV-1 Tat protein alters tight junction protein expression and distribution in cultured brain endothelial cells, J. Neurosci. Res. 74 (2003) 255–265.
[13] C. Ciobanasu, J.P. Siebrasse, U. Kubitscheck, Cell-penetrating HIV1 TAT peptides can generate pores in model membranes, Biophys. J. 99 (2010) 153–162.

[14] N. Khan, P.W. Halcrow, Z. Afghah, A. Baral, J.D. Geiger, X. Chen, HIV-1 Tat endocytosis and retention in endolysosomes affects HIV-1 Tat-induced LTR transactivation in astrocytes, Faseb. J. 36 (2022), e22184.
[15] N. Khan, P.W. Halcrow, L.K. Lakpa, M. Rehan, X. Chen, J.D. Geiger, Endolysosome iron restricts Tat-mediated HIV-1 LTR transactivation by increasing HIV-1 Tat oligomerization and beta-catenin expression, J. Neurovirol. 27 (2021) 755–773.
[16] A. Carocci, A. Catalano, M.S. Sinicropi, G. Genchi, Oxidative stress and neurodegeneration: the involvement of iron, Biometals 31 (2018) 715–735.
[17] S.M. Sadrzadeh, E. Graf, S.S. Panter, P.E. Hallaway, J.W. Eaton, Hemoglobin. A biologic fenton reagent, J. Biol. Chem. 259 (1984) 14354–14356.
[18] G. Papanikolaou, K. Pantopoulos, Iron metabolism and toxicity, Toxicol. Appl. Pharmacol. 202 (2005) 199–211.
[19] P. Arosio, R. Ingrassia, P. Cavadini, Ferritins: a family of molecules for iron storage, antioxidation and more, Biochim. Biophys. Acta 1790 (2009) 589–599.
[20] M.A. Knovich, J.A. Storey, L.G. Coffman, S.V. Torti, F.M. Torti, Ferritin for the clinician, Blood Rev. 23 (2009) 95–104.
[21] J.R. Boelaert, G.A. Weinberg, E.D. Weinberg, Altered iron metabolism in HIV infection: mechanisms, possible consequences, and proposals for management, Infect. Agents Dis. 5 (1996) 36–46.
[22] P.W. Halcrow, K.L. Lakpa, N. Khan, Z. Afghah, N. Miller, G. Datta, X. Chen, J. D. Geiger, HIV-1 gp120-induced endolysosome de-acidification leads to efflux of endolysosome iron, and increases in mitochondrial iron and reactive oxygen species, J. Neuroimmune Pharmacol. 17 (2022) 181–194.
[23] N. Khan, X. Chen, J.D. Geiger, Role of divalent cations in HIV-1 replication and pathogenicity, Viruses 12 (2020).
[24] A. Savarino, G.P. Pescarmona, J.R. Boelaert, Iron metabolism and HIV infection: reciprocal interactions with potentially harmful consequences? Cell Biochem. Funct. 17 (1999) 279–287.
[25] A.R. Kallianpur, H. Gittleman, S. Letendre, R. Ellis, J.S. Barnholtz-Sloan, W. S. Bush, R. Heaton, D.C. Samuels, D.R. Franklin Jr., D. Rosario-Cookson, D. B. Clifford, A.C. Collier, B. Gelman, C.M. Marra, J.C. McArthur, J.A. McCutchan, S. Morgello, I. Grant, D. Simpson, J.R. Connor, T. Hulgan, C.S. Group, Cerebrospinal fluid ceruloplasmin, haptoglobin, and vascular endothelial growth factor are associated with neurocognitive impairment in adults with HIV infection, Mol. Neurobiol. 56 (2019) 3808–3818.
[26] P. Bozzatello, C. Blua, P. Rocca, S. Bellino, Mental Health in childhood and adolescence: the role of polyunsaturated fatty acids, Biomedicines 9 (2021).
[27] Custers, E.M. Emma, Kiliaan, J. Amanda, Dietary lipids from body to brain, Prog. Lipid Res. 85 (2022), 101144.
[28] Q. Leyrolle, F. Decoeur, C. Dejean, G. Briere, S. Leon, I. Bakoyiannis, E. Baroux, T. L. Sterley, C. Bosch-Bouju, L. Morel, C. Amadieu, C. Lecours, M.K. St-Pierre, M. Bordeleau, V. De Smedt-Peyrusse, A. Sere, L. Schwendimann, S. Gregoire, L. Bretillon, N. Acar, C. Joffre, G. Ferreira, R. Uricaru, P. Thebault, P. Gressens, M. E. Tremblay, S. Laye, A. Nadjar, N-3 PUFA deficiency disrupts oligodendrocyte maturation and myelin integrity during brain development, Glia 70 (2022) 50–70.
[29] L. Mezzaroba, D.F. Alfieri, A.N. Colado Simao, E.M. Vissoci Reiche, The role of zinc, copper, manganese and iron in neurodegenerative diseases, Neurotoxicology 74 (2019) 230–241.
[30] S.K. Sharma, M.P. Bansal, R. Sandhir, Altered dietary selenium influences brain iron content and behavioural outcomes, Behav. Brain Res. 372 (2019), 112011.
[31] L. Gagnon, A.F. Smith, D.A. Boas, A. Devor, T.W. Secomb, S. Sakadzic, Modeling of cerebral oxygen transport based on in vivo microscopic imaging of microvascular network structure, blood flow, and oxygenation, Front. Comput. Neurosci. 10 (2016) 82.
[32] K. Masamoto, K. Tanishita, Oxygen transport in brain tissue, J. Biomech. Eng. 131 (2009), 074002.
[33] H. Esterbauer, R.J. Schaur, H. Zollner, Chemistry and biochemistry of 4-hydroxynonenal, malonaldehyde and related aldehydes, Free Radic. Biol. Med. 11 (1991) 81–128.
[34] A. Ayala, M.F. Munoz, S. Arguelles, Lipid peroxidation: production, metabolism, and signaling mechanisms of malondialdehyde and 4-hydroxy-2-nonenal, Oxid. Med. Cell. Longev. 2014 (2014), 360438.
[35] T.G. Nam, Lipid peroxidation and its toxicological implications, Toxicol. Res. 27 (2011) 1–6.
[36] G.C. Forcina, S.J. Dixon, GPX4 at the crossroads of lipid homeostasis and ferroptosis, Proteomics 19 (2019), e1800311.
[37] H. Liang, Q. Ran, Y.C. Jang, D. Holstein, J. Lechleiter, T. McDonald-Marsh, A. Musatov, W. Song, H. Van Remmen, A. Richardson, Glutathione peroxidase 4 differentially regulates the release of apoptogenic proteins from mitochondria, Free Radic. Biol. Med. 47 (2009) 312–320.
[38] K. Muthukumar, S. Rajakumar, M.N. Sarkar, V. Nachiappan, Glutathione peroxidase3 of Saccharomyces cerevisiae protects phospholipids during cadmium-induced oxidative stress, Antonie Leeuwenhoek 99 (2011) 761–771.
[39] P.S. Ogunro, T.O. Ogungbamigbe, M.O. Ajala, B.E. Egbewale, Total antioxidant status and lipid peroxidation in HIV-1 infected patients in a rural area of south western Nigeria, Afr. J. Med. Med. Sci. 34 (2005) 221–225.
[40] L. Agrawal, J.P. Louboutin, B.A. Reyes, E.J. Van Bockstaele, D.S. Strayer, HIV-1 Tat neurotoxicity: a model of acute and chronic exposure, and neuroprotection by gene delivery of antioxidant enzymes, Neurobiol. Dis. 45 (2012) 657–670.
[41] J. Huang, R. Zhang, S. Wang, D. Zhang, C.K. Leung, G. Yang, Y. Li, L. Liu, Y. Xu, S. Lin, C. Wang, X. Zeng, J. Li, Methamphetamine and HIV-tat protein synergistically induce oxidative stress and blood-brain barrier damage via transient receptor potential melastatin 2 channel, Front. Pharmacol. 12 (2021), 619436.
[42] A.V. Ivanov, V.T. Valuev-Elliston, O.N. Ivanova, S.N. Kochetkov, E. S. Starodubova, B. Bartosch, M.G. Isaguliants, Oxidative stress during HIV infection: mechanisms and consequences, Oxid. Med. Cell. Longev. 2016 (2016), 8910396.
[43] C.B. Pocernich, R. Sultana, H. Mohmmad-Abdul, A. Nath, D.A. Butterfield, HIV-dementia, Tat-induced oxidative stress, and antioxidant therapeutic considerations, Brain Res Brain Res Rev 50 (2005) 14–26.
[44] T.O. Price, N. Ercal, R. Nakaoke, W.A. Banks, HIV-1 viral proteins gp120 and Tat induce oxidative stress in brain endothelial cells, Brain Res. 1045 (2005) 57–63.
[45] P. Periyasamy, A. Thangaraj, V.S. Bendi, S. Buch, HIV-1 Tat-mediated microglial inflammation involves a novel miRNA-34a-NLRC5-NFkappaB signaling axis, Brain Behav. Immun. 80 (2019) 227–237.
[46] P. Periyasamy, A. Thangaraj, M.L. Guo, G. Hu, S. Callen, S. Buch, Epigenetic promoter DNA methylation of miR-124 promotes HIV-1 tat-mediated microglial activation via MECP2-STAT3 Axis, J. Neurosci. 38 (2018) 5367–5383.
[47] A. Thangaraj, P. Periyasamy, K. Liao, V.S. Bendi, S. Callen, G. Pendyala, S. Buch, HIV-1 TAT-mediated microglial activation: role of mitochondrial dysfunction and defective mitophagy, Autophagy 14 (2018) 1596–1619.
[48] A.N. Carey, E.I. Sypek, H.D. Singh, M.J. Kaufman, J.P. McLaughlin, Expression of HIV-Tat protein is associated with learning and memory deficits in the mouse, Behav. Brain Res. 229 (2012) 48–56.
[49] D.T. Chemparthy, M. Kannan, L. Gordon, S. Buch, S. Sil, Alzheimer's-Like pathology at the crossroads of HIV-associated neurological disorders, Vaccines 9 (2021).
[50] A. Cota-Gomez, N.C. Flores, C. Cruz, A. Casullo, T.Y. Aw, H. Ichikawa, J. Schaack, R. Scheinman, S.C. Flores, The human immunodeficiency virus-1 Tat protein activates human umbilical vein endothelial cell E-selectin expression via an NF-kappa B-dependent mechanism, J. Biol. Chem. 277 (2002) 14390–14399.
[51] J. Gorwood, T. Ejlalmanesh, C. Bourgeois, M. Mantecon, C. Rose, M. Atlan, D. Desjardins, R. Le Grand, B. Feve, O. Lambotte, J. Capeau, V. Bereziat, C. Lagathu, SIV infection and the HIV proteins tat and nef induce senescence in adipose tissue and human adipose stem cells, resulting in adipocyte dysfunction, Cells 9 (2020).
[52] A.N. Qrareya, F. Mahdi, M.J. Kaufman, N.M. Ashpole, J.J. Paris, HIV-1 Tat promotes age-related cognitive, anxiety-like, and antinociceptive impairments in female mice that are moderated by aging and endocrine status, Geroscience 43 (2021) 309–327.
[53] T. Wang, Z. Jiang, W. Hou, Z. Li, S. Cheng, L.A. Green, Y. Wang, X. Wen, L. Cai, M. Clauss, Z. Wang, HIV Tat protein affects circadian rhythmicity by interfering with the circadian system, HIV Med. 15 (2014) 565–570.
[54] B. Kenkhuis, A. Somarakis, L. de Haan, O. Dzyubachyk, I.J. Me, N. de Miranda, B. P.F. Lelieveldt, J. Dijkstra, W.M.C. van Roon-Mom, T. Hollt, L. van der Weerd, Iron loading is a prominent feature of activated microglia in Alzheimer's disease patients, Acta Neuropathol Commun 9 (2021) 27.
[55] B. Kenkhuis, M. van Eekeren, D.A. Parfitt, Y. Ariyurek, P. Banerjee, J. Priller, L. van der Weerd, W.M.C. van Roon-Mom, Iron accumulation induces oxidative stress, while depressing inflammatory polarization in human iPSC-derived microglia, Stem Cell Rep. 17 (2022) 1351–1365.
[56] A.A. Kapralov, Q. Yang, H.H. Dar, Y.Y. Tyurina, T.S. Anthonymuthu, R. Kim, C. M. St Croix, K. Mikulska-Ruminska, B. Liu, I.H. Shrivastava, V.A. Tyurin, H. C. Ting, Y.L. Wu, Y. Gao, G.V. Shurin, M.A. Artyukhova, L.A. Ponomareva, P. S. Timashev, R.M. Domingues, D.A. Stoyanovsky, J.S. Greenberger, R. K. Mallampalli, I. Bahar, D.I. Gabrilovich, H. Bayir, V.E. Kagan, Redox lipid reprogramming commands susceptibility of macrophages and microglia to ferroptotic death, Nat. Chem. Biol. 16 (2020) 278–290.
[57] R.F. Fernandez, J.M. Ellis, Acyl-CoA synthetases as regulators of brain phospholipid acyl-chain diversity, Prostaglandins Leukot. Essent. Fatty Acids 161 (2020), 102175.
[58] T.M. Lewin, J.H. Kim, D.A. Granger, J.E. Vance, R.A. Coleman, Acyl-CoA synthetase isoforms 1, 4, and 5 are present in different subcellular membranes in rat liver and can be inhibited independently, J. Biol. Chem. 276 (2001) 24674–24679.
[59] T.M. Lewin, C.G. Van Horn, S.K. Krisans, R.A. Coleman, Rat liver acyl-CoA synthetase 4 is a peripheral-membrane protein located in two distinct subcellular organelles, peroxisomes, and mitochondrial-associated membrane, Arch. Biochem. Biophys. 404 (2002) 263–270.
[60] H. Kuwata, S. Hara, Role of acyl-CoA synthetase ACSL4 in arachidonic acid metabolism, Prostag. Other Lipid Mediat. 144 (2019), 106363.
[61] G. Lei, Y. Zhang, P. Koppula, X. Liu, J. Zhang, S.H. Lin, J.A. Ajani, Q. Xiao, Z. Liao, H. Wang, B. Gan, The role of ferroptosis in ionizing radiation-induced cell death and tumor suppression, Cell Res. 30 (2020) 146–162.
[62] Q. Li, S. Guo, C. Yang, X. Liu, X. Chen, J. He, C. Tong, Y. Ding, C. Peng, Y. Geng, X. Mu, T. Liu, F. Li, Y. Wang, R. Gao, High-fat diet-induced obesity primes fatty acid beta-oxidation impairment and consequent ovarian dysfunction during early pregnancy, Ann. Transl. Med. 9 (2021) 887.
[63] X.F. Qu, T.Y. Liang, D.G. Wu, N.S. Lai, R.M. Deng, C. Ma, X. Li, H.Y. Li, Y.Z. Liu, H.T. Shen, G. Chen, Acyl-CoA synthetase long chain family member 4 plays detrimental role in early brain injury after subarachnoid hemorrhage in rats by inducing ferroptosis, CNS Neurosci. Ther. 27 (2021) 449–463.
[64] J. Quan, A.M. Bode, X. Luo, ACSL family: the regulatory mechanisms and therapeutic implications in cancer, Eur. J. Pharmacol. 909 (2021), 174397.
[65] W. Wang, X. Hao, L. Han, Z. Yan, W.J. Shen, D. Dong, K. Hasbargen, S. Bittner, Y. Cortez, A.S. Greenberg, S. Azhar, F.B. Kraemer, Tissue-specific ablation of ACSL4 results in disturbed steroidogenesis, Endocrinology 160 (2019) 2517–2528.

[66] X. Zhao, Y. Fan, P.H. Vann, J.M. Wong, N. Sumien, J.J. He, Long-term HIV-1 tat expression in the brain led to neurobehavioral, pathological, and epigenetic changes reminiscent of accelerated aging, Aging Dis 11 (2020) 93–107.
[67] H.C. Chang, M. Bayeva, B. Taiwo, F.J. Palella Jr., T.J. Hope, H. Ardehali, Short communication: high cellular iron levels are associated with increased HIV infection and replication, AIDS Res. Hum. Retrovir. 31 (2015) 305–312.
[68] L. Festa, C.J. Gutoskey, A. Graziano, B.D. Waterhouse, O. Meucci, Induction of interleukin-1beta by human immunodeficiency virus-1 viral proteins leads to increased levels of neuronal ferritin heavy chain, synaptic injury, and deficits in flexible attention, J. Neurosci. 35 (2015) 10550–10561.
[69] P.W. Halcrow, N. Kumar, Z. Afghah, J.P. Fischer, N. Khan, X. Chen, O. Meucci, J. D. Geiger, Heterogeneity of ferrous iron-containing endolysosomes and effects of endolysosome iron on endolysosome numbers, sizes, and localization patterns, J. Neurochem. 161 (2022) 69–83.
[70] S. Sil, G. Hu, K. Liao, F. Niu, S. Callen, P. Periyasamy, H.S. Fox, S. Buch, HIV-1 Tat-mediated astrocytic amyloidosis involves the HIF-1alpha/lncRNA BACE1-AS axis, PLoS Biol. 18 (2020), e3000660.
[71] K. Liao, M. Guo, F. Niu, L. Yang, S.E. Callen, S. Buch, Cocaine-mediated induction of microglial activation involves the ER stress-TLR2 axis, J. Neuroinflammation 13 (2016) 33.
[72] P. Periyasamy, K. Liao, Y.H. Kook, F. Niu, S.E. Callen, M.L. Guo, S. Buch, Cocaine-mediated downregulation of miR-124 activates microglia by targeting KLF4 and TLR4 signaling, Mol. Neurobiol. 55 (2018) 3196–3210.
[73] A. Thangaraj, E.T. Chivero, A. Tripathi, S. Singh, F. Niu, M.L. Guo, P. Pillai, P. Periyasamy, S. Buch, HIV TAT-mediated microglial senescence: role of SIRT3-dependent mitochondrial oxidative stress, Redox Biol. 40 (2021), 101843.
[74] J.P. Koelmel, W.Y. Tan, Y. Li, J.A. Bowden, A. Ahmadireskety, A.C. Patt, D. J. Orlicky, E. Mathe, N.M. Kroeger, D.C. Thompson, J.A. Cochran, J.P. Golla, A. Kandyliari, Y. Chen, G. Charkoftaki, J.D. Guingab-Cagmat, H. Tsugawa, A. Arora, K. Veselkov, S. Kato, Y. Otoki, K. Nakagawa, R.A. Yost, T.J. Garrett, V. Vasiliou, Lipidomics and redox lipidomics indicate early stage alcohol-induced liver damage, Hepatol Commun 6 (2022) 513–525.
[75] P. Periyasamy, A. Thangaraj, M. Kannan, A. Oladapo, S. Buch, The epigenetic role of miR-124 in HIV-1 tat- and cocaine-mediated microglial activation, Int. J. Mol. Sci. 23 (2022), 15017.
[76] P.P. Pillai, M. Kannan, S. Sil, S. Singh, A. Thangaraj, E.T. Chivero, R.S. Dagur, A. Tripathi, G. Hu, P. Periyasamy, S. Buch, Involvement of lncRNA TUG1 in HIV-1 tat-induced astrocyte senescence, Int. J. Mol. Sci. 24 (2023) 4330.
[77] J. Wang, J. Xu, Q. Wang, R.E. Brainard, L.J. Watson, S.P. Jones, P.N. Epstein, Reduced cardiac fructose 2,6 bisphosphate increases hypertrophy and decreases glycolysis following aortic constriction, PLoS One 8 (2013), e53951.
[78] A. Reinert, M. Morawski, J. Seeger, T. Arendt, T. Reinert, Iron concentrations in neurons and glial cells with estimates on ferritin concentrations, BMC Neurosci. 20 (2019) 25.
[79] H. Xie, K. Ma, K. Zhang, J. Zhou, L. Li, W. Yang, Y. Gong, L. Cai, K. Gong, Cell-cycle arrest and senescence in TP53-wild type renal carcinoma by enhancer RNA-P53-bound enhancer regions 2 (p53BER2) in a p53-dependent pathway, Cell Death Dis. 12 (2021) 1.
[80] J.P. Louboutin, L. Agrawal, B.A. Reyes, E.J. Van Bockstaele, D.S. Strayer, Oxidative stress is associated with neuroinflammation in animal models of HIV-1 tat neurotoxicity, Antioxidants 3 (2014) 414–438.
[81] A. Sapkota, J.W. Choi, Oleanolic acid provides neuroprotection against ischemic stroke through the inhibition of microglial activation and NLRP3 inflammasome activation, Biomol Ther (Seoul) 30 (2022) 55–63.
[82] W.S. Sheng, S. Hu, C.C. Hegg, S.A. Thayer, P.K. Peterson, Activation of human microglial cells by HIV-1 gp41 and Tat proteins, Clin. Immunol. 96 (2000) 243–251.
[83] J.Y. Lee, W.K. Kim, K.H. Bae, S.C. Lee, E.W. Lee, Lipid metabolism and ferroptosis, Biology 10 (2021).
[84] E. Soupene, V. Serikov, F.A. Kuypers, Characterization of an acyl-coenzyme A binding protein predominantly expressed in human primitive progenitor cells, J. Lipid Res. 49 (2008) 1103–1112.
[85] Y. Cui, Y. Zhang, X. Zhao, L. Shao, G. Liu, C. Sun, R. Xu, Z. Zhang, ACSL4 exacerbates ischemic stroke by promoting ferroptosis-induced brain injury and neuroinflammation, Brain Behav. Immun. 93 (2021) 312–321.
[86] S. Doll, B. Proneth, Y.Y. Tyurina, E. Panzilius, S. Kobayashi, I. Ingold, M. Irmler, J. Beckers, M. Aichler, A. Walch, H. Prokisch, D. Trumbach, G. Mao, F. Qu, H. Bayir, J. Fullekrug, C.H. Scheel, W. Wurst, J.A. Schick, V.E. Kagan, J.P. Angeli, M. Conrad, ACSL4 dictates ferroptosis sensitivity by shaping cellular lipid composition, Nat. Chem. Biol. 13 (2017) 91–98.
[87] L. Yang, F. Ye, J. Liu, D.J. Klionsky, D. Tang, R. Kang, Extracellular SQSTM1 exacerbates acute pancreatitis by activating autophagy-dependent ferroptosis, Autophagy (2022) 1–12.
[88] T.M. Seibt, B. Proneth, M. Conrad, Role of GPX4 in ferroptosis and its pharmacological implication, Free Radic. Biol. Med. 133 (2019) 144–152.
[89] L.A. Herzenberg, S.C. De Rosa, J.G. Dubs, M. Roederer, M.T. Anderson, S.W. Ela, S.C. Deresinski, L.A. Herzenberg, Glutathione deficiency is associated with impaired survival in HIV disease, Proc. Natl. Acad. Sci. U. S. A. 94 (1997) 1967–1972.
[90] S.M. Anderson, R.N. Naidoo, Y. Pillay, C. Tiloke, S. Muttoo, K. Asharam, A. A. Chuturgoon, HIV induced nitric oxide and lipid peroxidation, influences neonatal birthweight in a South African population, Environ. Int. 121 (2018) 1–12.
[91] A. Favier, C. Sappey, P. Leclerc, P. Faure, M. Micoud, Antioxidant status and lipid peroxidation in patients infected with HIV, Chem. Biol. Interact. 91 (1994) 165–180.
[92] L.I. Kolesnikova, M.A. Darenskaya, S.I. Kolesnikov, L.A. Grebenkina, M. A. Rashidova, E.V. Timofeeva, O.Y. Leshenko, O.A. Nikitina, Evaluation of lipid peroxidation processes in patients with chronic parenteral viral hepatitis and HIV co-infection depending on degree of inflammatory process activity in the liver, Ter. Arkh. 90 (2018) 37–43.
[93] M. Roederer, S.W. Ela, F.J. Staal, L.A. Herzenberg, L.A. Herzenberg, N-acetylcysteine: a new approach to anti-HIV therapy, AIDS Res. Hum. Retrovir. 8 (1992) 209–217.
[94] A.M. Battaglia, R. Chirillo, I. Aversa, A. Sacco, F. Costanzo, F. Biamonte, Ferroptosis and cancer: mitochondria meet the "iron maiden" cell death, Cells 9 (2020).
[95] M. Gao, J. Yi, J. Zhu, A.M. Minikes, P. Monian, C.B. Thompson, X. Jiang, Role of mitochondria in ferroptosis, Mol. Cell. 73 (2019) 354–363 e353.
[96] A. Cumaoglu, A.O. Agkaya, Z. Ozkul, Effect of the lipid peroxidation product 4-hydroxynonenal on neuroinflammation in microglial cells: protective role of quercetin and monochloropivaloylquercetin, Turk J Pharm Sci 16 (2019) 54–61.
[97] B. Yang, R. Li, C. Michael Greenlief, K.L. Fritsche, Z. Gu, J. Cui, J.C. Lee, D. Q. Beversdorf, G.Y. Sun, Unveiling anti-oxidative and anti-inflammatory effects of docosahexaenoic acid and its lipid peroxidation product on lipopolysaccharide-stimulated BV-2 microglial cells, J. Neuroinflammation 15 (2018) 202.
[98] W. Reid, M. Sadowska, F. Denaro, S. Rao, J. Foulke Jr., N. Hayes, O. Jones, D. Doodnauth, H. Davis, A. Sill, P. O'Driscoll, D. Huso, T. Fouts, G. Lewis, M. Hill, R. Kamin-Lewis, C. Wei, P. Ray, R.C. Gallo, M. Reitz, J. Bryant, An HIV-1 transgenic rat that develops HIV-related pathology and immunologic dysfunction, Proc. Natl. Acad. Sci. U. S. A. 98 (2001) 9271–9276.
[99] N.F. Homji, X. Mao, E.F. Langsdorf, S.L. Chang, Endotoxin-induced cytokine and chemokine expression in the HIV-1 transgenic rat, J. Neuroinflammation 9 (2012) 3.
[100] C.L. Nemeth, E.R. Glasper, C.S. Harrell, S.A. Malviya, J.S. Otis, G.N. Neigh, Meloxicam blocks neuroinflammation, but not depressive-like behaviors, in HIV-1 transgenic female rats, PLoS One 9 (2014), e108399.
[101] S.A. Rowson, C.S. Harrell, M. Bekhbat, A. Gangavelli, M.J. Wu, S.D. Kelly, R. Reddy, G.N. Neigh, Neuroinflammation and behavior in HIV-1 transgenic rats exposed to chronic adolescent stress, Front. Psychiatr. 7 (2016) 102.
[102] M. Vigorito, K.P. Connaghan, S.L. Chang, The HIV-1 transgenic rat model of neuroHIV, Brain Behav. Immun. 48 (2015) 336–349.
[103] J.C. Delpech, S. Herron, M.B. Botros, T. Ikezu, Neuroimmune crosstalk through extracellular vesicles in Health and disease, Trends Neurosci. 42 (2019) 361–372.
[104] A. Matejuk, R.M. Ransohoff, Crosstalk between astrocytes and microglia: an overview, Front. Immunol. 11 (2020) 1416.
[105] J. Rostami, T. Mothes, M. Kolahdouzan, O. Eriksson, M. Moslem, J. Bergstrom, M. Ingelsson, P. O'Callaghan, L.M. Healy, A. Falk, A. Erlandsson, Crosstalk between astrocytes and microglia results in increased degradation of alpha-synuclein and amyloid-beta aggregates, J. Neuroinflammation 18 (2021) 124.
[106] M. Kannan, S. Singh, D.T. Chemparathy, A.A. Oladapo, D.Y. Gawande, S. M. Dravid, S. Buch, S. Sil, HIV-1 Tat induced microglial EVs leads to neuronal synaptodendritic injury: microglia-neuron cross-talk in NeuroHIV, Extracellular Vesicles and Circulating Nucleic Acids 3 (2022) 133–149.